Ocean carbon cycling during the past 130,000 years - a pilot study on inverse paleoclimate record modelling

Christoph Heinze[1,2,3], Babette Hoogakker[4], and Arne Winguth[5]

[1]Geophysical Institute, University of Bergen, Allégaten 70, 5007 Bergen, Norway
[2]Uni Climate, Uni Research, Allégaten 55, 5007 Bergen, Norway
[3]Bjerknes Centre for Climate Research, Bergen, Norway
[4]Department of Earth sciences, University of Oxford, South Parks Road, Oxford OX1 3AN, UK
[5]Earth and Environmental Sciences, University of Texas at Arlington, P.O. Box 19049 Arlington, TX 76019, USA

Correspondence to: Christoph Heinze (christoph.heinze@uib.no)

Abstract. What role did changes in marine carbon cycle processes and calcareous organisms play for glacial-interglacial variation in atmospheric pCO_2? In order to answer this question, we explore results from an ocean biogeochemical ocean general circulation model. We make an attempt to systematically reconcile model results with time dependent sediment core data from the observations. For this purpose, simulated sensitivities of oceanic tracer concentrations to changes in governing carbon cycle parameters are fitted to measured sediment core data. We assume that the time variation of the governing carbon cycle parameters follows the general pattern of the glacial-interglacial deuterium anomaly. Our analysis provides an independent estimate of a maximum mean sea surface temperature drawdown of about 5°C and a maximum outgassing of the land biosphere by about 430 PgC at the last glacial maximum as compared to preindustrial times. The overall fit of modelled paleoclimate tracers to observations, however, remains quite weak indicating the potential of more detailed modelling studies for full exploitation of the information as stored in the paleo-climatic archive. It can be confirmed, however, that a decline in ocean temperature and a more efficient biological carbon pump in combination with changes in ocean circulation are the key factors for explaining the glacial CO_2 drawdown. The analysis suggests that potential changes in the export rain ratio POC:$CaCO_3$ may not have a substantial imprint on the paleo-climatic archive. The use of the last glacial as an inverted analogue to potential ocean acidification impacts thus may be quite limited. A potential strong decrease in $CaCO_3$ export production could contribute to the glacial CO_2 decline in the atmosphere but remains hypothetical.

1   Introduction

Since the mid-1980's the drawdown of the atmospheric CO_2 mixing ration from 280-290 ppm to 180 ppm is known from analysis of Antarctic ice core measurements (Neftel et al. (1982), Barnola et al. (1987), Siegenthaler et al. (2005)). Despite a series of attempts to explain this major fluctuation in the key atmospheric greenhouse gas CO_2, an overall closed explanation is still missing (Broecker and Peng (1986); Heinze et al. (1991); Heinze and Hasselmann (1993); Archer and Maier-Reimer (1994); Sigman and Boyle (2000); Archer et al. (2000); Brovkin et al. (2007)). An understanding of the positive feedback between climate and atmospheric CO_2 content (cf. Shakun et al. (2012)) is important also for quantifying the changing carbon

cycle today. The glacial-interglacial CO_2 variations are mainly caused by a redistribution of carbon between the Earth system reservoirs ocean, atmosphere, and land. In contrast, the modern carbon cycle is perturbed by the addition of CO_2 to the Earth's surface reservoirs, which had been excluded from interaction with biogeochemical processes in these reservoirs for a long time. Nevertheless, a reliable reconstruction of glacial-interglacial carbon dynamics with Earth system models would

5   enhance their predictability of future carbon cycle changes. The human-induced CO_2 emissions from fossil-fuel burning, cement manufacturing, and land-use change have risen the atmospheric CO_2 mixing ratio to 400 ppm relative to a pre-industrial level of 278 ppm (Le Quéré et al. (2014)). The atmospheric CO_2 mixing ration would be considerably higher, if the ocean would not take up a part of the human-made excess CO_2 from the atmosphere, primarily through physico-chemical buffering (Bolin and Eriksson (1959); Maier-Reimer and Hasselmann (1987); Joos et al. (2013)). This marine CO_2 buffering has the side

10   effect of reducing the seawater pH (Haugan and Drange (1996); Caldeira and Wickett (2003)). The impact of this progressing ocean acidification on marine biota, ecosystems, and biogeochemical processes is subject to broad interdisciplinary research and harmful effects could be identified (Raven (2005); Gattuso and Hansson (2011)). Especially a reduction in the formation of calcium carbonate ($CaCO_3$) shell material is at the focus of ocean acidification impact research (Riebesell et al. (2007); Iglesias-Rodriguez et al. (2008)). Several potential geologic analogues for oceaan acidification have been suggested (during the

15   Paleocene Eocene Thermal Maximum at 56 Ma, Zachos et al. (2005); CO_2 from the Siberian Traps Large Igneous Province, Svensen et al. (2009); methane release from magmatic intrusion into coal beds, Retallack (2008)). E.g., lack of sedimentary information prior to 180 million years before present limit the information about ecosystems back in deep time. Another prominent example of significant carbon fluctuations is the last glacial interglacial cycle. For example, the lower CO_2 partial pressure at the last glacial maximum (LGM) around 21 kyr BP (21,000 years before present) - could be used as a reverse paleo-

20   analogue to a high CO_2 world. Could we say anything about the average behaviour of marine biota with respect to $CaCO_3$ formation under glacial conditions in order to learn about possible future developments? Evidence for a better preservation of foraminifera shells is provided by Barker and Elderfield (2002) which would be in line with higher glacial carbonate ion concentrations in surface waters Yu et al. (2014).

In this study, we combine a coarse resolution biogeochemical ocean general circulation model (BOGCM) together with long

25   sediment core record time series in order to determine the most likely change in ocean carbon cycle parameters during the past climatic cycle. We include also the "rain ratio" $CaCO_3$:Corg (carbon atoms bound to $CaCO_3$ shell material versus carbon atoms bound to organic carbon in biogenic particulate matter during biological production) in the analysis. Thus, information is provided on whether the $CaCO_3$ formation in the glacial low CO_2 world increased or not. A $CaCO_3$ production increase at the LGM would be consistent with a decrease of $CaCO_3$ formation in a high CO_2 world. The model simulates a time dependent

30   sediment record at each model grid point for variations of single parameters over the past 130 kyr (see section 2). We determine the resulting model sensitivities for the sediment core tracers in relation to a number of key governing parameters of the ocean carbon cycle (see section 3). The sensitivities are projected onto a linear response model. This simplified model is then used for a simultaneous fit of all carbon cycle parameters to available sediment core data from the observed paleo-climatic archive (section 4). We pursue a multi-tracer approach by considering data on marine $CaCO_3$ wt-%, BSi wt-% (BSi is biogenic silica

35   or opal, rf. Ragueneau et al. (2000)), $\delta^{13}C_{planktonic}$, $\delta^{13}C_{benthic}$, and the atmospheric CO_2 record of the Vostok ice core

(Barnola et al. (1987); the EPICA Dome C ice core data will be used to define the sensitivity experiments which are used as input to the linear response model, see below).

2 Model description

We here use the Hamburg Oceanic Carbon Cycle Model *HAMOCC* (Maier-Reimer (1993); Maier-Reimer et al. (2005)), in its
5 annually averaged version ("HAMOCC2s") in order to keep the computational effort for equilibrating the sediment coverage in feasible limits (Heinze and Maier-Reimer (1999); Heinze et al. (1999); Heinze et al. (2003); Heinze et al. (2009)). This bio-geochemical ocean model requires as input three-dimensional velocity and thermohaline fields as well as ice cover data. For the spin-up of the model, a velocity field representing the pre-industrial conditions ("interglacial first guess", Winguth et al. (1999)) with an annually averaged circulation from the Large Scale Geostrophic dynamical ocean general circulation model
10 (Maier-Reimer et al. (1993)) is employed. The effect of deep convective mixing at high latitudes is considered in this forcing, which is used for transporting the passive tracer substances within the model water column reservoir. The model has a horizontal resolution of $3.5^o \times 3.5^o$ while the vertical resolution decreases downward with 11 layers centred at 25, 75, 150, 250, 450, 700, 1000, 2000, 3000, 4000, and 5000 m. The bioturbated top sediment zone, the "sediment mixed layer" is structured into 10 layers which are separated by "downcore" interfaces at 0, 0.3, 0.6, 1.1, 1.6, 2.1, 3.1, 4.1, 5.1, 7.55, and 10 cm. The simplifying
15 assumption is made that no pore water reactions take place below 10 cm depth in the sediment (following Smith and Rabouille (2002); Boudreau (1997)). HAMOCC2s parameterises the processes air-sea gas exchange, biogenic particle export produc-tion out of the ocean surface layer, particle flux through the water column and particle degradation by remineralisation and re-dissolution, advection as well as mixing dissolved substances with the ocean velocity field, deposition of particulate matter on the sea floor, pore water chemistry and diffusion, advection of solid sediment components, bioturbation, and sediment ac-
20 cumulation (export out of the sediment mixed layer or "burial"). The general concept of the sediment model closely follows Archer et al. (1993).

For the present model configuration, the following tracer concentrations are used as prognostic variables: the atmosphere includes $^{12}CO_2$ (carbon dioxide), $\delta^{13}CO_2$, and O_2; the water column contains DIC (dissolved inorganic carbon), POC (partic-ulate organic carbon), DOC (dissolved organic carbon), $CaCO_3$ (calcium carbonate or particulate inorganic carbon) of ^{12}C and
25 ^{13}C, particulate organic phosphorus (POP), dissolved oxygen O_2, dissolved PO_4^{3-} as biolimiting nutrient, silicic acid $Si(OH)_4$ and opal (biogenic particulate silica BSi); and sediment processes include pore waters - the same dissolved substances as in the water column - as well as solid sediment with clay, $CaCO_3$, opal, organic carbon, and organic phosphorus.

The model has been described in detail before (Heinze et al. (1999); Heinze et al. (2003); Heinze et al. (2006)). Details about the process parameterisations are summarised in Appendix A. In contrast to previous model versions, the treatment of the in-
30 organic carbon chemistry was updated following the procedure as detailed in Dickson et al. (2007). As compared to the previ-ously used quantifications for the reaction constants for the dissociation of carbonic and boric acid according to Mehrbach et al. (1973), the solubility product for $CaCO_3$ after Ingle (1975), and the pressure dependencies of Edmond and Gieskes (1970), the model required only minor retuning in order to correctly predict the pre-industrial atmospheric pCO_2 of ca. 280 μatm. As

before, DIC and TAlk are used as "master tracers" from which the other derived inorganic carbon species such as the CO_3^{2-} concentration, the carbonate saturation, and the pH value are computed through a Newton-Raphson algorithm. A further extension of the model as presented in Heinze et al. (2009) is the introduction of separate fields for POP (particulate organic phosphorus), DOP (dissolved organic phosphorus), and solid organic phosphorous in the sediment mixed layer to allow for variable

5   stoichiometry ("Redfield ratios" C:P) in this study. The other ocean water column and pore water processes are represented through parameterisations as described for in earlier model versions

2.1 Transport of age information and passive tracers in the sediment

Next to the various solid sediment components, the model predicts also the age of each sediment component. The age of the amount of each component rained onto the model seafloor is set to the actual model time step. The age information is then

10   handed down into the model sediment layer as a passive tracer and this information transport is also depending on the pore water dissolution reactions, the deposition flux, the vertical sediment advection, and the bioturbation. Each solid sediment species has an own age tracer. The higher the sediment accumulation rate is the closer the age values of the four different sediment component ages are. For a schematic of the sediment model, please, see Heinze et al. (2009) (Figures 1 and 2 therein).

The model sediment model is initialised at age 0 with only clay sediment layers and then spun-up. During the progressing

15   integration, the model builds up its own biogenic sediment and clay sediment according to the dust deposition and the kinetic control of the continental inputs of nutrients, carbon, and alkalinity as prescribed through bulk numbers. Simultaneously with the sediment distribution, the age structure of each solid weight fraction is established. In equilibrium, the global sediment accumulation rates are a function of the continental input rates. The local sediment accumulation rates and sediment compositions are fully prognostic variables. In order to also "flush" the sediment mixed layer in low accumulation regions of the

20   world ocean, the model is spun-up for 100,000 years to achieve overall quasi-equilibrium (as documented by the stability of the atmospheric pCO_2 level and the asymptotic approach of the simulated globally integrated sediment accumulation rates to the globally prescribed continental matter input fluxes).

The model includes the cycling of ^{13}C. The observed foraminiferal $CaCO_3$ sediment record reflects δ^{13}C variations from both the surface and the deep waters (depending on the shell material analysis of the different surface and deep dwelling

25   species). As an extension to Heinze et al. (2009), the present model version also includes sedimentary benthic δ^{13}C. Normally, only the surface ocean δ^{13}C, i.e. the $\delta^{13}C_{planktonic}$ is included in the simulated $CaCO_3$ deposited onto the model top sediment layer and then treated subsequently during pore water reactions and sediment advection. The reason for this is that now explicit benthic production of foraminifera is realised in the model. Applying the basic concept of the passive age tracer treatment in the early diagenesis module, we also transport the $\delta^{13}C_{benthic}$ signal of the $CaCO_3$ fraction within the sediment mixed layer

30   (where we set the benthic solid δ^{13}C value for the depositing $CaCO_3$ material to the respective bottom water δ^{13}C of the model layer directly over the respective top sediment box). Thus, the following sedimentary variables included in the present model for direct comparison with values from sediment core analysis: the "foraminiferal" values of $\delta^{13}C_{planktonic}$, $\delta^{13}C_{benthic}$ (as the latter would be recorded in reality, e.g., by the foraminiferal species *Cibicidoides wuellerstorfi*, cf. Zahn et al. (1986)), and also their vertical difference $\Delta\delta^{13}C = \delta^{13}C_{planktonic} - \delta^{13}C_{benthic}$ as an indicator of the strength of the biological pump (or

the vertical nutrient gradient in the water column, see Shackleton and Pisias (1985). The model master tracers DIC and TAlk for the inorganic carbon cycle include the sum of ^{12}C and ^{13}C. Explicit ^{13}C concentrations are computed from the spin-up through the requirement that the pre-industrial atmospheric δ^{13}C value of -6.5 ‰. The continental input rate of ^{13}C and the corresponding output rate through sediment accumulation where iteratively determined, so that in the final model spin-up the

5   ^{12}C and ^{13}C are fully compatible with the pre-industrial δ^{13}C value.

2.2   Control run

Important global bulk numbers for the quasi-equilibrium state of the 100,000 yr long control run are given in Table 1. For illustration of the control performance, examples for the export production rates and the respective sediment components are provided in Figure 1. Meridional cross sections for dissolved inorganic phosphate, the carbonate ion concentration, and δ^{13}C

10   of total dissolved inorganic carbon are shown in Figure 2. The model is able to reproduce the major characteristics of global tracer distributions, with decreasing deep water carbonate ion concentrations and δ^{13} values as well as increasing phosphate concentrations from the Atlantic to the Pacific Ocean. Simulated tracer patterns appear to be more smoothed as compared to the observations because of the coarse spatial resolution of the model. The CaCO$_3$ sediment distribution in the northern Pacific Ocean may show somewhat too high CaCO$_3$ wt-% as compared with observations. Based on experience with previous

15   simulations, the CaCO$_3$ content of the sediment mixed layer appears to react quite sensitively to the degree of undersaturation and the redissolution rate constants chosen. Therefore, a slight overestimate of CaCO$_3$ sediment in the control run avoids for many grid points a potential complete dissolution of CaCO$_3$ during the sensitivity experiments.

3   Sensitivity experiments

In order to determine, how the governing process parameters of the carbon cycle changed from the cold low CO$_2$ world

20   to the warmer and higher CO$_2$ pre-industrial world, we first carried out a suite of sensitivity experiments with the full 3-D carbon cycle model. In each run, we change only one of the governing parameters in order to determine the respective change of the biogeochemical system. We are in particular interested in the respective change of the inorganic as well as organic carbon cycle and how these changes are imprinted onto the simulated paleo climatic record. In a previous study Heinze et al. (1991) had carried out sensitivity experiments with an earlier version of HAMOCC and also compared the results with data

25   from the observational paleo-climatic archive. The present study, however, differs significantly from the previous approach. In Heinze et al. (1991) only equilibrium responses of the biogeochemical state to instantaneous parameter changes (permanent switch from one of the control run configurations) were tested, the alternative velocity field used did not resemble the glacial ocean very well, and the model did not include an interactive early diagenesis sub-model (only interactive bulk sediment reservoirs which did not allow for varying total system inventories). The latter issue thus allowed only a comparison between

30   the modelled tracer values and sediment core derived "proxy data". Also the fixed total system inventory of carbon, nutrients, and alkalinity allowed a limited range of system changes. Already in the first study of HAMOCC including an interactive

diagenesis module by Archer and Maier-Reimer (1994) revealed the higher sensitivity of such a model configuration, as the water column tracer inventory could vary considerably more dynamically.

We first carried out a control run over the past 130,000 years re-starting from the standard spin-up of the model. This control run revealed the excellent mass conservation and also the almost drift free ^{13}C distributions in all reservoirs. Thereafter,

5 a series of simulations with perturbed model parameters were conducted by restarting from the same re-industrial control run. The runs were started from "Eemian" conditions which we assumed to be similar to first order to the pre-industrial state as resulting from the HAMOCC spin-up. We then scaled the various parameter perturbations with the δD temperature record of the EPOCA Dome C ice core project (Jouzel (2004)) assuming that all carbon cycle variations during the past climatic cycle are correlated with temperature or the rather similar temporal pattern of the atmospheric CO_2 variation. There

10 are uncertainties associated with this assumption, as the Antarctic air temperature record is a localised record and may not reflect global temperature change, and also because ocean temperatures may lag behind this signal. On the other hand, the local Antarctic δD temperature record is highly correlated with the global atmospheric pCO_2 signal (Siegenthaler et al. (2005); Barnola et al. (1987); Jouzel et al. (1987)). The seawater temperature change would probably not lag too long behind this signal if reasonably long time intervals are considered. Due to the close correlation between air temperature and atmospheric

15 pCO_2 over the past glacial-interglacial cycle, we cannot strictly discriminate between drivers for ocean and land carbon cycle changes coming from physical (temperature) and biogeochemical forcings (pCO_2, carbonate saturation, pH value), but have to justify this independently for the different parameters under investigation. For the sensitivity experiments, we selected the following governing model parameters of the carbon cycle: (1) The sea surface temperature for computation of the chemical and biological constants, (2) the release/uptake of carbon from/by the terrestrial biosphere, (3) the degradation rate constant

20 of POC in the water column, (4) the dissolution rate constant of BSi in the water column, (5) the export production rain ratio $CaCO_3$:POC, (6) the 3-D oceanic velocity field, (6) the glacial dust deposition and associated stimulation of biological export production, and (8) the Redfield ratio C:P.

These parameter changes are summarised in Figure 3 and Table 2 and further described more in detail below.

3.1 Sea surface temperature for computation of the chemical and biological constants

25 In this experiment, we reduced the sea surface temperature up to a maximum change of 5 K (with the consideration that the minimum temperature stays at or above the freezing point of sea water) only for the computation of the temperature dependent chemical and biological parameters in the model, which usually all have their fixed control run values. The effect on the CO_2 solubility is relatively strong accounting for ca. 12 ppm change in atmospheric pCO_2 for a 1 K change in sea water temperature (cf. Broecker and Peng (1986)). The 5 K change in temperature is approximately the maximum change that can be expected

30 on the basis of stable oxygen isotopes or other temperature indicators (e.g., Stute et al. (1995)).

3.2 Release/uptake of carbon from/by the terrestrial biosphere

Also variations in the land carbon cycle need to be properly taken into account for the overall pCO_2 signal in the atmosphere and the imprint of ^{13}C on the sedimentary record. We do not explicitly model the terrestrial carbon cycle in our experiment. Rather

we assume here, that the land biosphere would have a smaller net primary production (Hoogakker et al. (2016)) and standing biomass stock and hence provide a release of carbon to the atmosphere under colder and dryer conditions. The amplitude for biomass carbon loss from the land biosphere to the atmosphere was set to -500 PgC, which is on the more modest side of respective estimates from terrestrial paleo-climate records according to Crowley (1995). The reason for this choice is, that a

5   potentially increased storage of organic carbon under the ice sheets and at cold conditions (lower bacterial activity for plant biomass degradation) is also being discussed (e.g., Zeng (2003)). Such storage could lower the overall carbon loss from the terrestrial biosphere under glacial conditions.

3.3   Dissolution rate constants of POC and BSi

We explored the temperature effect on both sinking particulate organic carbon as well as biogenic silica. We assumed that the

10   degradation of both substances slows down under lower temperatures due to thermodynamic effects as well as decreasing bacterial decomposition (Turley and Mackie (1995); Van Cappellen et al. (2002), Bidle and Azam (1999)). Through the respective parameter changes we tested separately a strengthening of the biological carbon and of the silicon pump which would have led to a deeper penetration of carbon and nutrients into the water column under glacial conditions ("vertical fractionation" as described by Boyle (1988a) and Boyle (1988b)). We chose a maximum decrease of degradation strength of 10%.

15   ### 3.4   Export production rain ratio CaCO$_3$:POC

A decrease in rain ratio has been suggested as one of the potential mechanisms to extract carbon from the atmosphere during glacial times (Berger and Keir (1984)). A reduction of the CaCO$_3$ production to zero could potentially explain half of the glacial pCO$_2$ drawdown from the atmosphere (Broecker and Peng (1986)). However, the experiments by Zondervan et al. (2001) and Riebesell et al. (2000) would suggest the opposite: In a low CO$_2$ world, the CaCO$_3$:POC ratio would be expected to decrease.

20   This would make it more difficult to explain the glacial CO$_2$ uptake by the oceans. Heinze and Hasselmann (1993) showed that this in principle is possible. We follow in our experiment here, however, the idea of an diminished CaCO$_3$:POC export production rain ratio during glacial times. In order to get a pronounced signal, we decrease the amplitude to a -10% change at the LGM with respect to the control run.

3.5   3-D oceanic velocity field

25   Practically all geochemically relevant paleoclimate tracers in the ocean depend on the ocean circulation. Therefore, it is necessary to take a realistic glacial velocity field into account in order to provide the correct addition to tracer changes which may be induced by biological and chemical processes. We follow here the same approach as outlined in Heinze (2001), where we "mix" the velocity, thermohaline, convective mixing, as well as sea ice margin values from two different runs of the dynamical ocean general circulation model LSG (Large Scale Geostrophic Model, Maier-Reimer et al. (1993)). These runs are the re-

30   spective interglacial and glacial first guess runs from Winguth et al. (1999) which show major features of the pre-industrial as well as LGM distributions of the δ^{13}C of dissolved inorganic carbon. As maximum amplitude for the velocity field change we

assume a full switch to LGM conditions at the largest negative excursion of the δD EPICA Dome C ice core curve. It would be preferable to have respective atmospheric forcing fields available to have physically better constrained velocity fields at hand. However, the considerable effort to realise such a run (which would need to be carried out with the full seasonally resolving LSG model) was deemed too large for our study here. The "kinematic" approach chosen here, should work for practical reasons

5   as the respective δ^{13}C distributions of DIC show realistic patterns.

3.6   Glacial dust deposition

We carried out a number of sensitivity tests concerning the effect of a change in continental dust deposition onto the sea surface. First we only tested the pure effect of clay addition through dust by applying the glacial dust deposition field by Mahowald et al. (1999) at the LGM and respective mixtures of interglacial and glacial dust deposition fields at other time

10   intervals. As the dust records of marine sediment core records usually do not follow the pattern of the δD record (e.g., Figure 4 of Carter and Manighetti (2006)), we scaled the change in dust supply with the 6th order of the glacial-interglacial difference of the δD curve, i.e. assumed a sudden increase of dustiness only at really low temperatures. Again we chose a maximum value of dust change to 100% glacial conditions at the LGM and smaller changes else (see Figure 3). The effect of this dust addition would be a change in the dilution of the sediment weight percentages of the reactive sedimentary material by inert

15   clay and also a change in the local sediment accumulation rates. It had been suggested that a stimulation of biological export production through increased dust and iron deposition to the ocean surface under glacial conditions (e.g., Martin et al. (1994); Berger and Wefer (1991)) could occur. In an additional experiment, the maximum uptake velocities for phosphorus, carbon, and silica were scaled with the glacial-interglacial difference of the dust deposition as provided by Mahowald et al. (1999). For the results of the fitting procedure as shown below, we considered here the run with the dilution effect only in order to separate

20   sediment dilution effects from those caused by an increase in biological production.

3.7   Redfield ratio C:P

Finally we allowed carbon over- or underconsumption in response to the interglacial to glacial change in environmental conditions. Riebesell et al. (2007) and Bellerby et al. (2008) postulated an increasing carbon overconsumption C:N under high CO_2 conditions resulting from a mesocosm experiment. In contrast, reversely, a change towards increasing carbon overcon-

25   sumption during the glacial low CO_2 world had been suggested as a powerful mechanism to account for the glacial CO_2 drawdown and at the same time cause a plausible foraminiferal δ^{13}C signal (e.g., Shackleton and Pisias (1985); Broecker (1982); Broecker and Peng (1986); Heinze and Hasselmann (1993)). In our sensitivity experiment we investigated the possibility for an increase in carbon overconsumption by imposing homogeneously over the ocean an increase in the Redfield ratio C:P. We specified a maximum change by 15% at the LGM (see Figure 3, lowermost panel).

30   We try to make a reasonable trade-off between the number of free parameters and the need for inclusion of the most essential parameters which contribute to the tracer variations in the paleo-record. Thus we aim at isolating imprints of parameter variations in the observed sedimentary record which would otherwise be masked by independent further processes (e.g., it could be

futile to derive changes in biological pump strength from the foraminiferal δ^{13}C distribution in the ocean without taking into account respective changes in the ocean currents which also affect the marine δ^{13}C distribution).

For determining the most likely choice of the governing parameters, we analysed modelled output for a series of paleo-climatic data sets. The model delivers first of all prognostic atmospheric pCO$_2$ values for each sensitivity experiment relative

5   to the control run during each time step for comparison with the Antarctic ice core records. The model runs were started from year 129536 BP and integrated until the present (the start year was chosen so that the first and last δD value are close to each other, no anthropogenic CO$_2$ emissions were imposed during the very last part of the integration). Each run requires around 4 days CPU time on an advanced UNIX work station. Using the methodology of Heinze et al. (2009) the model at each grid point accumulates sediment in a continuous way for the components CaCO$_3$, opal, organic carbon, clay, and organic

10   phosphorus. δ^{13}C$_{planktonic}$ and δ^{13}C$_{benthic}$ of the CaCO$_3$ fraction and the individual ages of each sediment component plus the atmospheric CO$_2$ partial pressure were stored together with the actual accumulation rates at the base of the sediment mixed layer. In order to reduce the amount of data output, we only stored 100-yr averages. Over the integration time period, for each run a continuous temporally varying sediment stratigraphy is built up. After the model runs, we "drill" into this synthetic sediment and "recover" simulated sediment cores for comparison with the observations from real world sediment core data.

15   We can provide such modelled cores at every grid point of the model individually.

4   Linear response model, observational sediment core data base, and fitting procedure

The inverse modelling procedure as applied and described here, draws in many aspects from the work by Heinze and Hasselmann (1993). We partly repeat some of the methodological issues here, to avoid that the reader has to refer too often to a separate study when reading this analysis here. The method is illustrated in Figure 4. We had carried out a total of eight sensitivity

20   experiments with the full 3-D biogeochemical ocean general circulation model, providing 8 different data sets for respective changes in 79 different tracer time series (see below) resulting formally in a total of 20,540 modelled tracer values and the same number of respective observed values (for each run). The eight sensitivity experiments represent the response of the full 3-D model for variations of n=8 governing input parameters x_j (j=1, …, n) (Table 2) resulting in m=20,540 paleoclimate tracer record changes g_i (i=1, …, m) as induced in these experiments as a consequence to the changes x_j of the parameters.

25   The resulting linear response model thus consists of the matrix describing the linearised relation between perturbations of the input and output variables. The model output variables $\hat{g}_i$ in the sensitivity experiments correspond to the observed perturbations of the atmospheric CO$_2$ record and the sediment records of CaCO$_3$, δ^{13}C$_{benthic}$, δ^{13}C$_{planktonic}$, and opal (BSi) (see following sub-section).

In the full non-linear biogeochemical ocean general circulation model, the paleo-climate tracers G_i are functions of the

30   governing model parameters X_j,

$$G_i \quad = \quad F_i(X_j) \quad . \tag{1}$$

In the simplified linear response model, the relation (1) is Taylor expanded (and then truncated) about a reference state $X_j = X_j^0$, $G_i = G_i^0$ as given by the defined by the standard run (with zero parameter changes):

$$\hat{g}_i = \sum_{j=1}^{n} A_{ij} x_j \qquad (2)$$

where $\hat{g}_i = G_i - G_i^0$, $x_j = X_j - X_j^0$ and $A_{ij} = \frac{\partial F_i}{\partial X_j}(X_j^0)$. The response coefficients A_{ij} form the elements of the model ma-
5 trix A. These response coefficients resulted from the model sensitivity experiments under the assumption of a linear relation between the parameter changes x_j and the response vector $\hat{g}_i$ predicted in every sensitivity experiment j.

4.1 Data base of observations from the paleo climate record

For calibrating the free model parameters, we employ a data base of paleo-climatic records as summarised in Tables 3 and 4. Locations are indicated in Figure 5. Most of the $\delta^{13}C_{benthic}$ and $\delta^{13}C_{planktonic}$ data were taken from the compilation of
10 Oliver et al. (2010). The majority of CaCO$_3$ wt-% data were taken from a compilation by Hoogakker (pers. comm., Table 4). Further marine sediment core data ($\delta^{13}C_{benthic}$, $\delta^{13}C_{planktonic}$, BSi, and CaCO$_3$ wt-%) were taken from various literature sources (see references in Tables 3 and 4). For atmospheric pCO$_2$ we use the Vostok ice core signal from Antarctica (Barnola et al. (1987)). We did not explicitly synchronise the different paleo-climatic time series to a common age model here, but rather took the measurement/age combinations at face value. We estimate the error due to this to up to a few thousand years
15 (compare the discussion in Oliver et al. (2010)). As we are not interested here in exact timing and phase shifts of signals in different variables, and due to the overall errors in the modelling approach (coarse resolution model, only crude representation of circulation changes, assumption that pre-industrial model state corresponds also to the Eemian) we assume that this approach is reasonable. Some sediment core data even were extracted from published graphics by hand. Most of the $\delta^{13}C_{benthic}$ and CaCO$_3$ wt-% time series employed, however, were synchronised in respective data compilations. For the fitting procedure, we
20 interpolated all observed data to regular time series with an increment of 500 years (260 equidistant data points in time).

Modelled annual global mean values of atmospheric pCO$_2$ were compared for comparison with the Vostok pCO$_2$ signal. The corresponding model time series data of the different sediment paleoclimate tracer curves where extracted for the various model sensitivity experiment runs from the respective model grid point closest to the location of real sediment core extraction. Modelled sediment data were interpolated with respect to age onto the same 500 years points as the observations. The age
25 of each sediment component was simulated according to Heinze et al. (2009) during the sensitivity experiments and stored together with the simulated depth in core of each modelled sediment variable.

For the fitting procedure, observed and modelled data where translated to changes relative to the preindustrial. Thus, we analysed the changes in the tracers relative to this reference while the respective parameter changes were taken as changes relative to the control run values.

4.2 Fitting procedure

Our general fitting procedure closely follows the method as described in Heinze and Hasselmann (1993)).

4.2.1 The general minimisation problem

We fitted the linearly modelled paleoclimatic tracer changes $\hat{g}_i$ to the observed tracer changes g_i through minimizing the mean square sum Q^2 of the individual tracer errors $\epsilon_i = \hat{g}_i - g_i$:

$$
\begin{aligned}
Q^2 &= \sum_{i=1}^{m} \epsilon_i^2 &= \sum_{i=1}^{m}(\sum_{j=1}^{n} A_{ij}\, x_j - g_i\,)^2 \\
&= (\cdot x^T{}_{\shortmid}\, {}_{\shortmid}A^T| - \cdot g^T|)\,(|A_{\shortmid}\, {}_{\shortmid}x\cdot - |g\cdot)
\end{aligned}
\tag{3}
$$

The dimensions of the vectors and matrices are described by the following symbols (cf. Heinze and Hasselmann (1993)): The left marker of a matrix symbol denotes the number of rows, the right marker specifies the number of columns. In our specific case, the marker "$\cdot$" corresponds to 1, "$|$" to the number $m = 20,540$ of observed tracer data, and "$_{\shortmid}$" to the number $n = 8$ of parameter changes x_j to be estimated. The solution ${}_{\shortmid}\hat{x}\cdot$ which minimizes the mean square expression Q^2 is derived through the necessary condition $\frac{dQ^2}{dx} = 0$:

$$
{}_{\shortmid}A^T|\,\, |A_{\shortmid}\,\, {}_{\shortmid}\hat{x}\cdot = {}_{\shortmid}A^T|\,\, |g\cdot
$$

which also can be written as

$$
{}_{\shortmid}\hat{x}\cdot = (\,{}_{\shortmid}A^T|\,\, |A_{\shortmid}\,)^{-1}\,{}_{\shortmid}A^T|\,\, |g\cdot
\tag{4}
$$

Through one realisation of the fitting procedure we thus, simultaneously, determined all eight optimal parameter changes $\hat{x}_j(t)$ necessary for a best possible reproduction of the observed tracer changes. In addition the procedure yields a time series of residual errors $\epsilon_i(t)$ which quantify the expected remaining discrepancies between modelled and observed tracers after the optimisation (we write here "expected" as the non-linear model may result in somewhat different residuals than the linear response model). Our problem is formally overdetermined where $m = 20540$ tracer data points must be fitted with must be fitted with $n = 8$ parameters. Therefore, the least squares formulation of our solution procedure is appropriate.

The error expression of eq. (3) is defined with a simple unit matrix norm. The more general maximum likelihood norm would be given by the inverse of the covariance matrix of the measurement errors (e.g., Martin (1971)). In eq. (3), we make the assumption that the errors are uncorrelated and have the same variance. At present, we have no conclusive means for estimating the error correlation. Therefore, the assumption of a simple unit matrix norm is reasonable here. However, we normalised the variables g_i by the mean absolute values of the respective tracer over the past climatic cycle, so that differential weighting of different tracer records, e.g., already from the use of different physical units is smoothed out.

4.2.2 The SVD least squares solution

In many inverse problems it is not possible to determine a physically meaningful least squares solution directly from eq. (4). The solution can be contaminated by noise if the model matrix $|A_{\shortmid}$ is badly conditioned. This leads in practice to unrealistically high variations of the optimised parameter changes if these depend only on very small variations in the tracer changes. Beforehand, it cannot be seen whether A is badly conditioned or not. Therefore, we applied the singular value decomposition (SVD)

technique which provides a quantitative treatment of the noise problem. For an introduction to this technique, please, see the very useful work by Wunsch (1989). The model matrix A is decomposed into a product of three matrices (SVD; see Lanczos (1961)):

$$|A| \quad = \quad |U| \; |\Lambda| \; |V^T|$$ (5)

5 The column vectors of $|U|$ and $|V|$ represent orthonormal bases $|u_i \cdot$, $i = 1, \ldots, m$ and $|v_j \cdot$, $j = 1, \ldots, n$ for the tracer (here tracer change) and parameter (here parameter change) spaces, respectively, associated with the model matrix $|A|$. $|\Lambda|$ The diagonal rectangular matrix

$$|\Lambda| \quad = \quad \begin{pmatrix} \lambda_1 & 0 & . & . & . & 0 \\ 0 & \lambda_2 & . & . & . & . \\ . & . & . & . & . & . \\ . & . & . & . & . & . \\ . & . & . & . & . & . \\ . & . & . & . & . & 0 \\ 0 & . & . & . & 0 & \lambda_n \\ 0 & . & . & . & . & 0 \\ . & . & . & . & . & . \\ 0_{1,m} & . & . & . & . & 0_{n,m} \end{pmatrix} .$$

consists of the singular values λ_k. The eigenvectors $|u_k \cdot$, $|v_k \cdot$ and the eigenvalues λ_k form the solution of the coupled eigenvalue

10 problem:

$$|A| \; |v_k \cdot \quad = \quad \lambda_k \; |u_k \cdot$$ (6)
$$|A^T| \; |u_k \cdot \quad = \quad \lambda_k \; |v_k \cdot$$ (7)

with the following properties:

$$|A| \; |A^T| \; |u_k \cdot \quad = \quad \lambda_k^2 \; |u_k \cdot$$ (8)
15 $$|A^T| \; |A| \; |v_k \cdot \quad = \quad \lambda_k^2 \; |v_k \cdot \; .$$ (9)

The number $p \le min(m, n)$ of non-zero singular values defines the rank of $|A|$.

The unknown parameter changes $|\hat{x} \cdot$ and the modelled tracer changes $|\hat{g} \cdot$ can now be written in terms of the linearly independent eigenvectors $|v_j \cdot$ and $|u_i \cdot$, respectively:

$$|\hat{x} \cdot \quad = \quad \sum_{j=1}^{p=n<m} \alpha_j \; |v_j \cdot$$ (10)

20 $$|\hat{g} \cdot \quad = (g_1, \ldots, g_m) = \quad \sum_{i=1}^{p=n<m} \beta_i \; |u_i \cdot$$ (11)

where the α_j are unknown and $\beta_i = \cdot u_i^T| \ |g\cdot$. The observed tracer changes are correspondingly given by $|g\cdot \equiv \sum_{i=1}^{m} \beta_i \ |u_i \ \cdot)$ Equations (4), (7), and (9) together yield the solution for the optimal parameter changes:

$$|\hat{x}\cdot \ = \ \sum_{j=1}^{n} \alpha_j \ |v_j \ \cdot \ = \ \sum_{i=1}^{n} \frac{1}{\lambda_i} \ |v_i\cdot \ \cdot u_i^T| \ |g\cdot \ . \tag{12}$$

with $\alpha_i = \beta_i/\lambda_i$. Because only $p = n < m$ vectors $|u_i\cdot$ are combined in the overdetermined case, residuals between mod-
5 elled tracer changes $|\hat{g}\cdot$ and observed tracer changes $|g\cdot$ occur. Thus, the observed tracer variations cannot be completely recombined by the least squares solution of eq. (12).

In the exactly determined case we would have

$$|\hat{g}\cdot \ \equiv \ |g\cdot \ = \ \sum_{i=1}^{m} \beta_i \ |u_i \ \cdot \ = \ \sum_{i=1}^{m} \ |u_i\cdot \ \cdot u_i^T| \ |g\cdot \ = \ |(\delta_{ij})| \ |g\cdot \tag{13}$$

where $\delta_{ij} = \begin{cases} 1 & for \quad i=j \\ 0 & for \quad i \neq j \end{cases}$.

10 For the overdetermined case we arrive at

$$|\hat{g}\cdot \ = \ \sum_{i=1}^{p=n<m} \beta_i \ |u_i \ \cdot \ = \ \sum_{i=1}^{p=n<m} \ |u_i\cdot \ \cdot u_i^T| \ |g\cdot \ = \ |\hat{U}| \ |\hat{U}^T| \ |g\cdot \ = \ |R_I| \ |g\cdot \tag{14}$$

with $|R_I| \ = \ |\hat{U}| \ |\hat{U}^T|$ being the "resolution matrix" (Wiggins (1972); Wunsch (1989)) of the changes in the tracer concentrations and $|\hat{U}| \ = \ (\ |u_1\cdot, \ldots, \ |u_n\cdot\ )$ is the truncated "model" version of the tracer base matrix $|U|$.

According to eq. (12), the coefficient α_i in the linear combination of the parameter space eigenvectors $|v_i \cdot$ grows to very
15 large values if λ_i becomes very small. These very small λ_i values lead to an unstable solution: Only unreasonable extremely large changes in selected parameters would be able to create the tracer changes as observed. The contributions to the solution from these small eigenvalues should accordingly be filtered out or considered with a significantly reduced weight.

For the resulting parameter changes from our fitting procedure, we discarded those components in eq. (12) associated with the smallest singular values step by step starting with the smallest singular value, followed by the next smallest one , and so
20 on) to filter out unrealistically large parameter changes. The associated approximate solution becomes then

$$|\hat{x}\cdot \ = \ \sum_{i=1}^{p<n} \frac{1}{\lambda_i} \ |v_i\cdot \ \cdot u_i^T| \ |g\cdot \tag{15}$$

The number p of eigenvalues retained is called the effective rank of $|A|$. In our case here the full rank solution would be achieved for a rank=8 (including all parameter changes). For an effective rank smaller than $min(m, n)$, the formally overdetermined problem is now changed into an underdetermined problem. Nevertheless solution eq. (15) is the unique least squares
25 solution with minimum length of the solution vector for the underdetermined case (e.g., Matsu'ura and Hirata (1982)). Such a solution with minimum overall change of the system under investigation often is physically or chemically seen the most appropriate solution ("Occam's razor").

Because the filtered solution relies on fewer fitted parameters changes, the goodness of fit of this filtered solution is poorer than in the full rank SVD solution. Because the rank p of the reduced matrix is smaller than the number of original param-
30 eters, the fitted parameters are no longer linearly independent. Now, one can specify only p linearly independent parameter

combinations. The full rank solution ($p = n \leq m$) would be:

$$\hat{x}_{full\ rank} = \sum_{j=1}^{p=n} \alpha_j v_j = \sum_{j=1}^{p=n} v_j \cdot v_j^T \hat{x}_{full\ rank} = (\delta_{ij}) \hat{x}_{full\ rank} \quad (16)$$

The solution for the rank deficient case ($p < n \leq m$) is now:

$$\hat{x} = \sum_{j=1}^{p<n} \alpha_j v_j = \sum_{j=1}^{p<n} v_j \cdot v_j^T \hat{x}_{full\ rank} = \hat{V} \hat{V}^T \hat{x}_{full\ rank}$$
$$= R_P \hat{x}_{full\ rank} \quad . \quad (17)$$

$R_P = \hat{V} \hat{V}^T$ is the "resolution matrix" of the parameters with $\hat{V} = (v_1, \ldots, v_p)$. This resolution matrix R_P projects the full (in art insufficiently constrained) set of parameters onto the sub-space of stable solutions for the parameter changes. If for fixed i the diagonal element R_{ii}^P of the matrix R_P is close to 1 and the other elements R_{ij}^P, $j \neq i$ are close to zero, parameter x_i is still well resolved even in the underdetermined case. Less well resolved parameters, are instead replaced by a stable linear combination of the original parameters. Through analysis of the resolution matrix for the parameters, we can therefore determine which parameter changes can be uniquely determined by the analysis and for which parameters no clear conclusion can be made.

5   Results and their discussion

We carried out numerous runs with the linear response model testing different combinations of parameters and observed time series of the paleoclimate as constraints. Overall we experienced, that the paleoclimatic information and the system sensitivity as provided by the biogeochemical ocean model lead to quite consistent results, if several parameters and paleoclimatic tracers are taken into account.

We present here results where we included all parameter changes and all paleoclimatic tracer curves (see summaries in Table 5 and Figures 6-8). The 8 unknowns (namely the excursions of the parameter amplitudes relative to interglacial conditions) where determined by an optimal fit to the 20,540 data points form the observational records. Formally, such a system is heavily overdetermined. No *a priori* knowledge and no artificial limits where imposed to the free parameters to be determined. Are the results for the free parameters reasonable? Figure 6 shows the parameter time series for the full rank solution (compare to the first guess values as shown in Figure 3), which also gives the best fit to the observations. Please, note that the model parameter changes by purpose show the same temporal pattern (special case dust as discussed above) and only the maximum amplitude of the parameters was determined. The *a posteriori* parameter changes remain relatively close to the initially chosen parameter changes (first guesses), yet with one exception. The rain ratio change shows a dramatic decrease in pelagic $CaCO_3$ production. Such a change may not be fully out of scope (see, e.g., the discussion in Broecker and Peng (1986)) but one would possibly expect rather an increase in $CaCO_3$ production at low ambient pCO_2 and high $CaCO_3$ saturation. The suggested strong change in the rain ratio may be an unstable part of the solution, where the fitting procedure needs huge changes in one (or possibly several parameters) to achieve minor changes in the paleoclimate tracers simulated. (Nevertheless, the corresponding SVD

solution is the unique solution of the system for full rank with altogether minimum deviation from the control run.) We, therefore, started to reduce the rank from 8 to first 7 and then 6, i.e. we still aimed at determining all 8 parameter changes simultaneously, but partially in linear combination of each other. In the solution for rank 7 (Figure 7), the change in sea surface temperature seems to be unrealistically high. A global decrease by about 8°C would imply an unrealistic widespread ocean

5 freezing. The solution for rank 6 (Figure 8) finally arrives at overall realistic parameter excursions during the past climatic cycle. As maximum changes at the LGM our analysis arrives at:

- A maximum decrease in global sea surface temperature by 5°,

- a decrease of the land biosphere by 400 PgC,

- only minor changes in POC and BSi degradation,

10 - a suggested change of the ocean velocities towards glacial conditions (no full switch however),

- an only small effect of dust deposition,

- and a sizable strengthening of the biological organic carbon pump through a stoichiometry change.

The resulting requirement for a strengthening of the biological pump could potentially also be due to other processes than a stoichiometry change in reality.

15 The suggested glacial drop in average SST by 5°C may still be overestimated. Originally, CLIMAP Project Members (1976) and Broecker (1986) estimated a glacial-interglacial change of only ca. -2.0°C to -2.3°C om faunal assemblages and oxygen isotopes, with the more recent quantification by MARGO Project Members (2009) being at the lower end of this range. Other estimates suggest a decline in the SST of 5.4°C Stute et al. (1995)) and even 6.5°C (Weyhenmeyer et al. (2000)). Green et al. (2002) arrive at an estimate for tropical SST glacial decrease of around 3°C but give a range of studies (see their Table 2 on p.

20 4-9 in Greene et al., 2002). Our study confirms through an independent approach the order of magnitude in this parameter.

A decrease in land vegetation due to colder and dryer climate conditions at the LGM relative to pre-industrial conditions has been estimated by several authors employing various approaches: 430 PgC (Shackleton (1977), 530-1160 PgC (Crowley (1995)), 330 PgC (Ciais et al. (2012)), and 597 PgC (O'ishi and Abe-Ouchi (2013)). Interestingly, our estimate is closest to the value originally determined by Shackleton (1977), which may be due to the marine δ^{13}C constraint used in that study which

25 also is included in our analysis. Overall, our study confirms earlier estimates on the LGM terrestrial carbon storage through an independent by our approach.

Our fitting procedure confirms that the glacial ocean circulation should have somehow resembled the simulated glacial ocean conditions as deduced by Winguth et al. (1999). However, in an ideal case with a perfect simulation of the glacial ocean circulation, the switch to this circulation at glacial conditions should be close to 100 % and not only 50 % as in this study.

30 This may be due to still some deviations of the simulated glacial ocean velocity especially for the Pacific Ocean, but also due to deficiencies in the biogeochemical model including its sediment module. Nevertheless, the tendency of a reaction towards glacial physical boundary conditions resulting from the fitting procedure is encouraging and consistent.

The most difficult part in interpreting the results are the reactions of the ecosystem parameters. The small changes in POC and BSi degradation or dissolution rates may be realistic in view of the overall still modest change in seawater temperatures. The almost vanishing rain ration change in the rank 6 solution and the suggested rain ratio decrease (corresponding to $CaCO_3$ export production decrease) cannot be easily explained. The lack of better information on $CaCO_3$ production during glacial times can here not give any clear answer concerning potential ocean acidification impacts. The reaction of the system during glacial times remains diffuse in our analysis (see also below for the resolution of parameters analysis).

For some $CaCO_3$ tracer records a remarkable improvement in fit resulted when employing increased dust deposition and the related dilution effect (not shown). However, on the average the inverse approach does not suggest a strong effect of the dust deposition changes for a better reproduction of the paleo-climate tracers here. This can possibly be due to the simple modelling approach which we take here and regional variations in dust deposition which so far cannot be resolved by the input fields.

The increase in carbon overconsumption (change in stoichiometry of carbon to nutrient elements) as suggested in our study confirms earlier results (Heinze and Hasselmann (1993)). This does not necessarily mean that such a change in carbon to nutrient ratio is realistic, at least for two reasons: Ecosystem changes to achieve such a change would need to be dramatic. The glacial-interglacial atmospheric CO_2 change corresponds in amplitude to about the pre-industrial to present increase. So far, no respective carbon underconsumption due to the anthropogenic CO_2 release has been identified. Rather, the opposite has been suggested for further dramatic increases in atmospheric and sea surface CO_2 (Riebesell et al. (2007)). The increase of carbon to nutrient ratios under cold and low-CO_2 conditions would contradict the evidence from mesocosm experiments in a Norwegian coastal setting (Riebesell et al. (2007)). The experimental results from the mesocosm studies may potentially be influenced by the specific experiment setting and thus may not be valid at other locations. Earlier, Heinze and Hasselmann (1993) could not well separate the effect of stimulation of POC export production by a change in stoichiometry or by an increase of the oceanic inventory of dissolved phosphate. Thus, the requirement of a carbon overconsumption in this study may indicate that the biological organic carbon production may have been stimulated by other processes than carbon overconsumption , e.g., fertilisation of ocean productivity by dust-derived micro-nutrients.

Moreover, we look at the impact of the rank reduction on the parameter change quantification and the goodness of fit to the observations. The reduction of the rank of our linear system involves that not all unknown parameter changes can be determined in an independent way. The resolution matrix of the parameters (cf. eq. 17 identifies which free parameters still can be uniquely determined after the rank reduction and which ones can only be given as linear combinations of each other.

Instead of giving the matrices in terms of numerical values, we visualised the matrices through circles in Figure 9, for the solution with rank 8 (full rank), rank 7, and rank 6. The full rank resolution diagram shows a perfect diagonal with all parameters formally perfectly resolved. For the rank reduction, the resolution for the rain ratio change, and also the BSi dissolution rate change deteriorates strongly. This shows, that the linear system is in fact poorly constrained, and that after all hardly anything can be firmly said about the glacial-interglacial rain ratio change. Unfortunately, implications for future ocean acidification impacts cannot be deduced from our analysis. This is important information, however. It may be that the quite comprehensive sediment record collection which we employed here, may still be inadequate to address the ocean acidification problem and possibly also the atmospheric glacial CO_2 draw-down problem. Parts of the real system may not be represented - being it in

the observations, in the model, or both. Further sedimentary tracer types may be needed in order to make the data base more complete and to resolve all and possible more carbon cycle parameters properly. The trade-off between realistic parameter estimates and goodness of fit becomes obvious when one checks, e.g., the overall estimated reproduction of the atmospheric Vostok ice core curve for the full rank and rank deficient solutions (Figure 10). While the full rank solution gives a quite

5 striking fit to the atmospheric CO_2 curve, already the rank 7 solution shows a strong decrease in fit, while finally the rank 6 solution (and thus also all solutions with smaller ranks) reveals an almost complete deterioration of the fit. This provides a clear dilemma.

In general, the improvement of the fit for a simultaneous optimisation of all parameters is quite weak except for atmospheric pCO_2 (see summary in Table 6). However, our 3-D biogeochemical ocean model is not detailed enough to capture all aspects of

10 the glacial ocean correctly. For example, our representation of the circulation variations is simplified. Also it may be possible that we have missed one or more key processes, which may have caused or contributed to the simultaneous changes in the paleo-climate tracer distributions. Further, we did not carry out any regional differentiation concerning the perturbation of governing parameters but used global mean changes. More detailed data assimilation schemes and the use of higher resolution coupled biogeochemical-physical models will be an option on the future for better reproducing the sediment core data, however, for the

15 price of many more degrees of freedom to constrain correctly. It remains a possibility, that the glacial biological $CaCO_3$ shell material production indeed was considerably smaller than the interglacial production in the case that this parameter change did not cause any major imprint on the paleo-climate tracer combination which was used in this study. In addition, also some of the sedimentary records may reflect specific local conditions which spatially cannot be resolved by our coarse model. Such special local conditions can include sediment focusing due to specific bathymetric features, smaller scale dynamic flow conditions

20 such as localised upwellings, and meandering frontal systems.

We also analysed the change in simulated tracer records as compared to the control run (Table 7). As one can see, in spite of the poor fit (except for the atmospheric pCO_2 record), indeed deviations from the tracer output records of the model control run occurred. These tend to get smaller with reduction of the rank.

6 Conclusions

25 In our study we combine a comprehensive sedimentary data base from the paleo-climatic sediment core record with a coarse resolution BOGCM. We assume that the governing carbon cycle parameter variations over the past climatic cycle follow the same temporal pattern. As the paleo-record of atmospheric pCO_2 and surface temperature show a strong correlation (Siegenthaler et al. (2005)), we cannot decide in general on whether the parameter variations are caused by physical forcing (temperature), chemical forcing (CO_2), or both simultaneously. With such approximation, we can reduce the search for un-

30 known parameter changes to the maximum amplitude of these changes at the LGM. By employing 79 observed paleo-climatic tracer data curves (with altogether 20,540 formal data points) for determination of 8 unknown maximum parameter excursions with respect to the preindustrial situation, we arrive at a formally completely overdetermined linear response model for esti-mating the parameter changes. We can confirm the quantification for mean global maximum SST change (-5 K) and carbon

loss from terrestrial systems (-430 PgC) to the atmosphere as suggested by earlier studies. Further, our model-data combination clearly identifies a substantial increase in the biological organic carbon export during glacial times, though the underlying process may not be a carbon to nutrient overconsumption. The response of glacial-interglacial changes in the biological $CaCO_3$ production remain uncertain. $CaCO_3$:C_{org} rain ratio reductions may have contributed to the glacial CO_2 reduction in the atmo-

5   sphere, but such rain ratio changes cannot be resolved with our linear response model. This can be due to model deficiencies in our approach, or due to lack of information from the present data base for this purpose. With our combination of model results and observations no overall answer concerning the mechanisms behind the glacial pCO_2 drawdown can be provided. Simple synchronous temperature dependent or atmospheric pCO_2 dependent forcing fields and governing parameter time series of the same temporal pattern appear to not be able to reproduce the marine sediment core record satisfactorily.

Data sets: The observational sediment core data sets have been taken from the literature. For the comprehensive compilation of $CaCO_3$ sediment core data, please, contact B. Hoogakker.

Appendix A: Model details

Major process parameterisations of the biogeochemical model used in this study are summarised below. The model is the

15   annually averaged version of the HAMOCC model (Maier-Reimer (1993); Maier-Reimer et al. (2005)) and has been described elsewhere (Heinze and Maier-Reimer (1999); Heinze et al. (1999); Heinze et al. (2003); Heinze et al. (2009)). Several free model parameters have been tuned anew for this study as compared to earlier studies. A number of important parameters are summarised in Table A1.

20   **Air-sea gas exchange**

The atmospheric model reservoirs atmosphere and ocean surface layer exchange CO_2 and oxygen. The flux of CO_2 across the air-sea interface is simulated as follows:

$$F_{CO2} \quad = \quad k_{CO2} \cdot (pCO_{2,air} - pCO_{2,water}) \tag{A1}$$

where F_{CO2} is the carbon dioxide flux across air/sea interface and k_{CO2} is the specific gas exchange rate. The CO_2 partial

25   pressure is calculated from the free carbon dioxide concentration (sum of aqueous CO_2 and carbonic acid) in seawater with Henry's law through use of the solubility α (Weiss (1974)):

$$pCO_{2,water} \quad = \quad \alpha \cdot [CO_2] \tag{A2}$$

For the oxygen flux the following approach is pursued:

$$F_{O2} = k_{O2} \cdot (C_{O2,equilibrium} - C_{O2,actual}) \tag{A3}$$

30    $$C_{O2,equilibrium} = f(T,S) \cdot C_{O2,atmosphere}(t)$$

where F_{O2} is the net gas flux between sea surface and atmosphere, k_{O2} is the mean gas transfer velocity, $C_{O2,equilibrium}$ and $C_{O2,actual}$ are the oceanic oxygen concentrations for solubility equilibrium with the atmosphere and the actual observed (or

modelled) value, $f(T,S)$ is the measured solubility as a function of sea water temperature and salinity, and $C_{O2,atmosphere}(t)$ is the tropospheric O_2 concentration, where $f(T,S)$ is taken from Weiss (1970). O_2 gas exchange is resulting from the analytical solution of the differential equation

$$\frac{dC}{dt} = F/\Delta z,$$

where C is the gas concentration in [mole/cm^3], F the flux in [mole(cm^2· s)] of gas into (or out of) a control volume of 1 cm length, 1cm width and thickness Δz in [cm]. The numerical formulation is

$$
\begin{aligned}
C^{new} &= C_{equilibrium} \\
&+ \left(C^{old} - C_{equilibrium}\right) \cdot e^{(-k_{av}/\Delta z)\cdot \Delta t}
\end{aligned}
\tag{A4}
$$

where Δt is the time step (here 1 year) and Δz is the thickness of the layer affected by gas exchange (Δz is set equal to 50 m in cases of hydrostatic stability and to the maximum depth of the convective layer else). The model atmosphere is represented through a 1 layer box over each grid point. At every time step, zonal averages are determined for the atmospheric concentrations. Gas transport is simulated through meridional diffusion only (as in reality the intrahemispheric tropospheric mixing time is much shorter than the time step of 1 year applied here).

Biogenic particle export production and particle flux through the water column

As a consequence of the annual averaging, the model simulates only export production of biogenic particles. Particle production is assumed to exclusively take place in the model surface layer representing the euphotic zone. Phosphate serves as ultimate biolimiting nutrient, the nitrogen cycle is not simulated explicitly. POC (particulate organic carbon) and opal export production rates are predicted using Michaelis Menten kinetics for nutrient uptake (e.g., Parsons and Takahashi (1973)):

$$P_{POC} = \frac{V_{max}^{POC} \cdot [PO_4^{3-}]^2 \cdot Red(C:P)}{K_s^{POC} + [PO_4^{3-}]} \tag{A5}$$

$$P_{opal} = \frac{V_{max}^{opal} \cdot [Si(OH)_4]^2}{K_s^{opal} + [Si(OH)_4]} \tag{A6}$$

where P_{POC} and P_{opal} are the POC and opal export production rates [molel^{-1} yr^{-1}], $Red(C:P)$ is the Redfield ratio C:P, V_{max}^{POC} and V_{max}^{opal} are the maximum uptake rate of phosphate and silicic acid from the water column [yr^{-1}], and K_s^{POC} as well as K_s^{opal} are the respective half saturation constants. The parameters V_{max}^{POC}, V_{max}^{opal}, K_s^{POC}, and K_s^{opal} are prescribed as a function of sea surface temperature following Heinze et al. (2003).

CaCO$_3$ export production depends on the local production ratio P_{opal}/P_{POC}. CaCO$_3$ export starts to gradually increase gradually when P_{opal}/P_{POC} sinks below a threshold value S_{opal}, i.e., when the silicic acid concentration is becoming too

small to support exclusively diatom growth:

$$P_{CaCO_3} = P_{POC} \cdot R \cdot (1 - \frac{P_{opal}/P_{POC}}{S_{opal}}), \tag{A7}$$

$$for \quad P_{opal}/P_{POC} < S_{opal};$$

$$P_{CaCO_3} = 0, \tag{A8}$$

$$for \quad P_{opal}/P_{POC} \geq S_{opal}$$

where R is the maximum possible rain ratio C(CaCO$_3$):C(POC) and S_{opal} is the threshold value of P_{opal}/P_{POC} for gradual onset of CaCO$_3$ production.

Particle fluxes and particle degradation are simulated through mass balance equations for sinking particulate matter M_{settle}, where M_{settle} stands for the different particle species POC_{settle}, $CaCO3_{settle}$, $opal_{settle}$, and $clay_{settle}$ respectively. The general formulation for the mass balance M_{settle} becomes then:

$$\frac{d\,M_{settle}}{dt} = gain - loss \tag{A9}$$

$$\frac{d\,M_{settle}}{dt} = P_M - \frac{w_M}{\Delta z_0} \cdot M_{settle} - r_M \cdot M_{settle}$$

$$(for \; surface \; layer)$$

$$\frac{d\,M_{settle}}{dt} = w_M \cdot \frac{\partial M_{settle}}{\partial z} - r_M \cdot M_{settle}$$

$$(for \; other \; layers)$$

where Δz_0 is the thickness of the euphotic zone [m], w_M is the particle settling velocity [m yr^{-1}], r_M is the reaction rate constant [yr^{-1}] for degradation of particulate matter, and P_M is the export production rate in the top layer, where again "M" denotes one of the particle species POC, CaCO$_3$, opal, and clay respectively. P_{clay} is the dust input from the atmosphere which is prescribed for the control run according to the modern dust deposition field from (Mahowald et al. (1999)). Clay material is considered as chemically inert. The system of equations (A9) is solved through an implicit numerical scheme. CaCO$_3$ dissolution in the water column is performed depending on the prevailing carbonate saturation using the following rate constant:

$$r_{CaCO3} = k_{CaCO3} \cdot (1 - \Omega) \tag{A10}$$

where k_{CaCO3} is a fixed standard rate constant, and $(1 - \Omega) = ([CO_3^{2-}]_{sat} - [CO_3^{2-}])/[CO_3^{2-}]_{sat}$ is the degree of undersaturation. Similar to Heinze et al. (2009) we apply a minimum value of 0.062 for the undersaturation thus allowing for some CaCO$_3$ dissolution in oversaturated waters (as a simplification our model simulates only calcite and not the meta-stable form aragonite or high Mg calcites). Opal dissolution is formulated to depend on the deviation from the saturation concentration for opal in seawater (following Ragueneau et al. (2000); where in the formulation below the effect of changes in free surface area of reactive opal is formally lumped into k_{opal} here):

$$r_{opal} = k_{opal} \cdot (Si_{saturation} - Si_{actual})/(1 \quad mole \quad l^{-1}) \tag{A11}$$

with k_{opal} a standard upper limit opal degradation rate, $Si_{saturation}$ the water column saturation value for silicic acid, and Si_{actual} the actual silicic acid value at a model grid point (the division by $1 mol e l^{-1}$ is needed in order to match the units correctly).

The losses in particulate matter according to eq. (A9) for settling particulate material are mirrored by respective source
5   terms for the dissolved species within the water column (for TAlk, DIC, phosphate, oxygen, and silicic acid). The remainder of particles which are not subject to degradation within the water column are deposited onto the top sediment layer (see sedimentary source term Q further below).

10 ## Sediment pore water chemistry and diffusion

Early diagenetic processes are simulated as described in Heinze et al. (2009), following the efficient numerical formulations of Maier-Reimer et al. (2005) for the implicit simultaneous treatment of porewater transport and porewater reactions as well as the vertical sediment advection. The porosity depth profile is fixed using numerical values of Ullman and Aller (1982). The basic sediment model concept is expressed through the equilibrium:

15    $sediment\ accumulation = deposition - redissolution$

The mass balance equations for a solid sediment component expressed in moles per unit volume of sediment S_* and the related concentration of the corresponding dissolved substance C within the pore water are:

$$\frac{dS_*}{dt} = D_B \frac{\partial^2 S_*}{\partial z^2} - \frac{\partial}{\partial z}(w \cdot S_*) - G \tag{A12}$$

$$\frac{dC}{dt} = \frac{\partial}{\partial z}(D_W \frac{\partial C}{\partial z}) + G \tag{A13}$$

20   where D_B is the diffusion coefficient for bioturbation, w the vertical advection velocity of solid compound, and G the reaction rate (with S_*, C, and G reported here in relation to full sediment volume of a given sediment layer for sake of simplicity; within the model, the varying volumes for dissolved and solid substances following the porosity profile are taken into account). The prognostic equations for solid sediment concentrations S_* (organic carbon, $CaCO_3$, opal, and clay) and for dissolved components C (TAlk, DIC, phosphate, oxygen, and silicic acid) are coupled through the respective reaction rates. The diffusive
25   transport of porewater tracer concentrations is simulated via the respective deviations from saturation in parallel with the reduction of this deviation due to chemical porewater reactions:

$$\frac{dU}{dt} = \frac{\partial}{\partial z}(D_W \frac{\partial U}{\partial z}) - G \tag{A14}$$

where U is the deviation of the saturation concentration C_{sat} from the actual concentration C) [mole l^{-1}], G is the reaction rate (sink for U from dissolution of solid material) [mole l^{-1} yr^{-1}] and D_W is the diffusion coefficient. As diffusion coefficient
30   D_W we employ a general value of $8\cdot 10^{-6}$ cm^2/s for all porewater tracers (this value is in the range of the values given for various pore water species in the work of Li and Gregory (1974). The solid sediment components change due to porewater reactions and particle deposition corresponding to eq. A14:

$$\frac{dS_*}{dt} = -G + Q \tag{A15}$$

where S_* is the solid sediment component expressed in the same units as U [mole l^{-1}], G is the reaction rate (sink due to dissolution) [mole l^{-1} yr^{-1}], and Q is the deposition flux from particle rain [mole l^{-1} yr^{-1}] (the latter occurs only in the top sediment layer). The amount G of solid matter which can be dissolved per unit of time is a function of parameter r_c^*, the deviation from saturation concentration U, and the amount of solid material available S_*:

$$G = r_c^* \cdot U \cdot S_* \tag{A16}$$

where for r_c^* we have:

$$r_c^* = \frac{r_c}{C_{sat}} \tag{A17}$$

with r_c being the reaction rate constant [yr^{-1}] and C_{sat} the saturation concentration in solution [mole l^{-1}]. For opal dissolution a solubility C_{sat} of 800 μmole l^{-1} is used [cf. Dixit et al. (2001), and for organic carbon a constant formal value of 100 μmole
10 l^{-1} is used (details of anaerobic respiration and respective effects such as denitrification and sulphate reduction are not taken explicitly into account). For the sedimentary CaCO$_3$, the CO$_3^{2-}$ saturation concentration is now also computed through the revised inorganic carbon system quantification following Dickson et al. (2007) (see eq. A10). The discretised versions of the coupled equations (A14 and A15) are solved implicitly through a numerical back-substitution formulation. Transport of dissolved tracers through porewater diffusion is not carried out as a boundary condition problem. Rather we formally include
15 the lowermost wet grid box in the water column directly over the model seafloor in the pore water diffusion scheme. Thus the free water column and the sediment pore waters directly exchange matter with each other.

Bioturbation

Bioturbation is simulated as in Heinze et al. (2009) through vertical "diffusion" of the solid substances. This step is carried
20 out after the vertical advection step described further below. The solid matter compounds are slowly mixed in proportion to the prevailing weight fractions in the layers overlying each other:

$$\frac{dS_*}{dt} = \frac{\partial}{\partial z}\left(D_B \frac{\partial S_*}{\partial z}\right) \tag{A18}$$

with D_B being the bioturbation coefficient. Non-local mixing (e.g., Boudreau and Imboden (1987)) is neglected here.

25 **Advection of solid sediment weight fractions and sediment accumulation** Vertical advection of sediment is performed as in Heinze et al. (2009), where the direction of sediment accumulation depends on the amount of the matter deposited onto the top sediment layer, and the re-dissolution rate of matter within the sediment mixed layer. The four different weight fractions clay, CaCO$_3$, opal, POC, and POP are shifted downward or upward according to the gain from the deposition flux and the gaps which are created from dissolution. In case of very strong corrosion in the bioturbated zone, only clay is transported
30 upward from below the sediment mixed layer. For an illustration of the mode of sediment advection for the different cases (a) burial > rain − redissolution (accumulation of sediment) and (b) burial < rain − (erosion of sediment), please, see Figure 2 in Heinze et al. (2009). The vertical sediment advection velocity w and also its sign (see eq. A12) depend on the sediment deposition from the water column and the strength of the pore water chemical reactions.

Acknowledgements. Thanks are due to many colleagues and friends. Ernst Maier-Reimer (Max Planck Institute for Meteorology) provided the basic HAMOCC model and crucial advice on efficient numerical modelling. Marion Gehlen and James Orr provided help for revising the model inorganic chemistry treatment for using the appropriate pH scale. Thanks are due to Natalie Mahowald for providing the dust deposition fields. Arne Winguth is supported by grant NSF-OCE 1536630. This work was partially supported through the University of Bergen (sabbatical funds for C. Heinze), through the "European Project on Ocean Acidification" (EPOCA; which received funding from the European Community's Seventh Framework Programme (FP7/2007-2013) under grant agreement n° 211384). The Research Council of Norway supported this study through the nationally coordinated project "Earth system modelling of climate variations in the Anthropocene" (EVA; grant no. 229771) as well as project "Overturning circulation and its implications for global carbon cycle in coupled models"(ORGANIC; grant no. 239965/RU). This is a contribution to the Bjerknes Centre for Climate Research (Bergen, Norway). A part of the computations where carried out under project NN2980K at the Norwegian Metacenter for Computational Science NOTUR and its dedicated storage and archiving project NorStore (NS2980k).

References

Archer, D. and Maier-Reimer, E.: Effect of deep-sea sedimentary calcite preservation on atmospheric CO_2 concentration, Nature, 367, 260–263, doi:10.1038/367260a0, 1994.

Archer, D., Lyle, M., Rodgers, K., and Froelich, P.: What controls opal preservation in tropical deep-sea sediments, Paleoceanography, 8, 7–21, doi:10.1029/92PA02803, 1993.

Archer, D., Winguth, A., and andN Mahowald, D. L.: What caused the glacial/interglacial atmospheric pCO(2) cycles?, Reviews of geophysics, 38, 159–189, doi:10.1029/1999RG000066, 2000.

Barker, S. and Elderfield, H.: Foraminiferal calcification response to glacial-interglacial changes in atmospheric CO2., Science, 297, 833–6, doi:10.1126/science.1072815, 2002.

Barnola, J., Raynaud, D., Korotkevich, Y., and Lorius, C.: Vostok ice core provides 160,000-year record of atmospheric CO_2, Nature, 329, 408–414, doi:10.1038/329408a0, 1987.

Becquey, S. and Gersonde, R.: Past hydrographic and climatic changes in the Subantarctic Zone of the South Atlantic - The Pleistocene record from ODP Site 1090, Palaeogeography, Palaeoclimatology, Palaeoecology, 182, 221–239, doi:10.1016/S0031-0182(01)00497-7, 2002.

Becquey, S. and Gersonde, R.: A 0.55-Ma paleotemperature record from the Subantarctic zone: Implications for Antarctic Circumpolar Current development, Paleoceanography, 18, doi:10.1029/2000PA000576, 2003.

Bellerby, R., Schulz, K., Riebesell, U., Neill, C., Nondal, G., Heegaard, E., Johannessen, T., and Brown, K.: Marine ecosystem community carbon and nutrient uptake stoichiometry under varying ocean acidification during the PeECE III experiment, Biogeosciences, 5, 1517–1527, doi:10.5194/bg-5-1517-2008, 2008.

Berger, W. and Keir, R.: Glacial-Holocene Changes in Atmospheric CO_2 and the Deep-Sea Record, pp. 337–351, American Geophysical Union, Washington, D.C., doi:10.1029/GM029p0337, j.E. Hansen and T. Takahashi (Eds.), Geophysical Monograph 29, 1984.

Berger, W. and Wefer, G.: Productivity of the glacial ocean - discussion of the iron hypothesis, Limnology and oceanography, 36, 1899–1918, doi:10.4319/lo.1991.36.8.1899, 1991.

Bickert, T.: Rekonstruktion der spätquartären Bodenwasserzirkulation im östlichen Südatlantik über stabile Isotope benthischer Foraminiferen, Berichte, Fachbereich Geowissenschaften, Universität Bremen, 27, 205 pp, 1992.

Bickert, T. and Mackensen, A.: Last Glacial to Holocene changes in South Atlantic deep water circulation, pp. 671–695, Springer-Verlag, Berlin, Heidelberg, New York, Tokyo, G Wefer and S Mulitza and S Ratmeyer (Eds.), 1996.

Bickert, T. and Wefer, G.: Late Quaternary deep water circulation in the South Atlantic: Reconstruction from carbonate dissolution and benthic stable isotopes, pp. 599–620, Springer-Verlag, Berlin, g Wefer and WH Berger and G Siedler and D Webb (Eds.), 1996.

Bidle, K. and Azam, F.: Accelerated dissolution of diatom silica by marine bacterial assemblages, Nature, 397, 508–512, doi:10.1038/17351, 1999.

Bolin, B. and Eriksson, E.: Changes in the carbon dioxide content of the atmosphere and sea due to fossil fuel combustion, pp. 130–142, Rockefeller Inst., New York, B. Bolin (Ed.), Rossby memorial volume, 1959.

Boudreau, B.: Diagenetic models and their implementation: modelling transport and reactions in aquatic sediments, Springer, Berlin and Heidelberg, 414 p., 1997.

Boudreau, B. and Imboden, D.: Mathematics of tracer mixing in sediments. 3. The theory of nonlocal mixing within sediments, American Journal of Science (1818-1819), 287, 693–719, doi:10.2475/ajs.287.7.693, 1987.

Boyle, E.: Vertical oceanic nutrient fractionation and glacial interglacial CO_2 cycles, Nature, 331, 55–56, doi:10.1038/331055a0, 1988a.

Boyle, E.: Glacial interglacial deep ocean circulation contrast, Chemical geology, 70, 108–108, doi:10.1016/0009-2541(88)90504-9, 1988b.

Broecker, W.: Ocean chemistry during glacial time, Geochimica et cosmochimica acta, 46, 1689–1705, doi:10.1016/0016-7037(82)90110-7, 1982.

Broecker, W.: Oxygen isotope constraints on surface ocean temperatures, Quaternary research, 26, 121–134, doi:10.1016/0033-5894(86)90087-6, 1986.

Broecker, W. and Peng, T.: Carbon cycle - 1985 Glacial to interglacial changes in the operation of the global carbon cycle, Radiocarbon, 28, 309–327, 1986.

Brovkin, V., Ganopolski, A., Archer, D., and Rahmstorf, S.: Lowering of glacial atmospheric CO2 in response to changes in oceanic circulation and marine biogeochemistry, Paleoceanography, 22, doi:10.1029/2006PA001380, 2007.

Caldeira, K. and Wickett, M. E.: Oceanography: anthropogenic carbon and ocean pH., Nature, 425, 365–365, doi:10.1038/425365a, 2003.

Carter, L. and Manighetti, B.: Glacial/interglacial control of terrigenous and biogenic fluxes in the deep ocean off a high input, collisional margin: A 139 kyr-record from New Zealand, Marine geology, 226, 307–322, doi:10.1016/j.margeo.2005.11.004, 2006.

Carter, L., Manighetti, B., Ganssen, G., and Northcote, L.: Southwest Pacific modulation of abrupt climate change during the Antarctic Cold Reversal - Younger Dryas, Palaeogeography, Palaeoclimatology, Palaeoecology, 260, 284–298, doi:10.1016/j.palaeo.2007.08.013, 2008.

Charles, C., Froelich, P., Zibello, M., Mortlock, R., and Morley, J.: Biogenic opal in southern ocean sediments over the last 450,000 years: implications for surface water chemistry and circulation, Paleoceanography, 6, 697–728, doi:10.1029/91PA02477, 1991.

Chuey, J., Rea, D., and Pisias, N.: Late Pleistocene Paleoclimatology of the central equatorial Pacific - a quantitative record of eolian and carbonate deposition, Quaternary research, 28, 323–339, doi:10.1016/0033-5894(87)90001-9, 1987.

Ciais, P., Tagliabue, A., Cuntz, M., Bopp, L., Scholze, M., Hoffmann, G., Lourantou, A., Harrison, S., Prentice, I., Kelley, D., Koven, C., and Piao, S.: Large inert carbon pool in the terrestrial biosphere during the Last Glacial Maximum, Nature geoscience, 5, 74–79, doi:10.1038/NGEO1324, 2012.

CLIMAP Project Members: The surface of the ice-age Earth, Science, 191, 1131–1137, 1976.

Crowley, T.: Ice-age terrestrial carbon changes revisited, Global biogeochemical cycles, 9, 377–389, doi:10.1029/95GB01107, 1995.

Curry, W. and Oppo, D.: Synchronous, high-frequency oscillations in tropical sea surface temperatures and North Atlantic Deep Water production during the last glacial cycle, Paleoceanography, 12, 1–14, doi:10.1029/96PA02413, 1997.

Curry, W., Duplessy, J., Labeyrie, L., and Shackleton, N.: Changes in the distribution of δ^{13}C of deep water ΣCO_2 between the last glaciation and the Holocene, Paleoceanography, 3, 317–341, doi:10.1029/PA003i003p00317, 1988.

Dickson, A., Sabine, C., and Christian, J., eds.: Guide to best practices for ocean CO_2 measurements, North Pacific Marine Science Organization, Sidney BC, Canada, PICES Special Publication 3, IOCCP Report No. 8, 191 p., 2007.

Dixit, S., Van Cappellen, P., and van Bennekom, A.: Processes controlling solubility of biogenic silica and pore water build-up of silicic acid in marine sediments, Marine chemistry, 73, 333–352, doi:10.1016/S0304-4203(00)00118-3, 2001.

Dürkop, A., Hale, W., Mulitza, S., Pätzold, J., and Wefer, G.: Late Quaternary variations of sea surface salinity and temperature in the western tropical Atlantic: Evidence from delta O-18 of Globigerinoides sacculifer, Paleoceanography, 12, 764–772, doi:10.1029/97PA02270, 1997.

Edmond, J. and Gieskes, J.: On the calculation of the degree of saturation of sea water with respect to calcium carbonate under in situ conditions, Geochimica et Cosmochimica Acta, 34, 1261–1291, doi:doi:10.1016/0016-7037(70)90041-4, 1970.

Freudenthal, T.: Reconstruction of productivity gradients in the Canary Island Region off Morocco by means of sinking particles and sediments, Berichte, Fachbereich Geowissenschaften, Universität Bremen, 165, 147 pp., 1998.

Freudenthal, T., Meggers, H., Henderiks, J., Kuhlmann, H., Moreno, A., and Wefer, G.: Upwelling intensity and filament activity off Morocco during the last 250,000 years, Deep-sea research. Part 2, Topical studies in oceanography, 49, 3655–3674, doi:10.1016/S0967-0645(02)00101-7, 2002.

Gattuso, J. and Hansson, L., eds.: Ocean acidification, Oxford University Press, New York, 326 pp., 2011.

Haugan, P. and Drange, H.: Effects of CO2 on the ocean environment, Energy conversion and management, 37, 1019–1022, doi:10.1016/0196-8904(95)00292-8, 1996.

Heinze, C.: Towards the time dependent modeling of sediment core data on a global basis, Geophysical Research Letters, 28, 4211–4214, doi:10.1029/2001GL013479, 2001.

Heinze, C. and Hasselmann, K.: Inverse multiparameter modeling of paleoclimate carbon cycle indices, Quaternary research, 40, 281–296, doi:10.1006/qres.1993.1082, 1993.

Heinze, C. and Maier-Reimer, E.: The Hamburg Oceanic Carbon Cycle Circulation Model Version "HAMOCC2s" for long time integrations, Tech. rep., Max Planck Institute for Meteorology, Hamburg, Germany, Series: Technical Reports, no. 20, ISSN 0940-9327, 1999.

Heinze, C., Maier-Reimer, E., and Wynn, K.: Glacial pCO_2 reduction by the world ocean: Experiments with the Hmburg carbon cycle model, Paleoceanography, 6, 395–430, doi:10.1029/91PA00489, 1991.

Heinze, C., Maier-Reimer, E., Winguth, A., and Archer, D.: A global oceanic sediment model for long-term climate studies, Global biogeochemical cycles, 13, 221–250, doi:10.1029/98GB02812, 1999.

Heinze, C., Hupe, A., EMaier-Reimer, Dittert, N., and Ragueneau, O.: Sensitivity of the marine biospheric Si cycle for biogeochemical parameter variations, Global biogeochemical cycles, 17, doi:10.1029/2002GB001943, 2003.

Heinze, C., Gehlen, M., and Land, C.: On the potential of Th-230, Pa-231, and Be-10 for marine rain ratio determinations: A modeling study, Global biogeochemical cycles, 20, doi:10.1029/2005GB002595, 2006.

Heinze, C., Kriest, I., and Maier-Reimer, E.: Age offsets among different biogenic and lithogenic components of sediment cores revealed by numerical modeling, Paleoceanography, 24, doi:10.1029/2008PA001662, 2009.

Hodell, D.: Late Pleistocene paleoceanography of the South Atlantic sector of the Southern Ocean: Ocean Drilling Program Hole 704A, Paleoceanography, 8, 47–67, doi:10.1029/92PA02774, 1993.

Hodell, D., Charles, C., Curtis, J., Mortyn, P., Ninnemann, U., and Venz, K.: Data Report: Oxygen isotope stratigraphy of ODP Leg 117 sites 1088, 1089, 1090, 1093, and 1094, pp. 1–26, ODP, College Station, TX, doi:doi:10.2973/odp.proc.sr.177.120.2003, R. Gersonde, D.A. Hodell and P. Blum (Eds.), 2003a.

Hodell, D., Venz, K., Charles, C., and Ninnemann, U.: Pleistocene vertical carbon isotope and carbonate gradients in the South Atlantic sector of the Southern Ocean, Geochemistry, geophysics, geosystems, 4, doi:10.1029/2002GC000367, 2003b.

Hoogakker, B., Smith, R., Singarayer, J., Marchant, R., Prentice, I., Allen, J., Anderson, R., Bhagwat, S., Behling, H., Borisova, O., Bush, M., Correa-Metrio, A., de Vernal, A., Finch, J., Fréchette, B., Lozano-Garcia, S., Gosling, W., Granoszewski, W., Grimm, E., Grüger, E., Hanselman, J., Harrison, S., Hill, T., Huntley, B., Jiménez-Moreno, G., Kershaw, P., Ledru, M., Magri, D., McKenzie, M., Müller, U., Nakagawa, T., Novenko, E., Penny, D., Sadori, L., Scott, L., Stevenson, J., Valdes, P., Vandergoes, M., Velichko, A., Whitlock, C., and Tzedakis, C.: Terrestrial biosphere changes over the last 120 kyr, Climate of the past, 12, 51–73, doi:doi:10.5194/cp-12-51-2016, 2016.

Howard, W. and Prell, W.: Late Quaternary surface circulation of the southern Indian Ocean and its relationship to orbital variations, Paleoceanography, 7, 79–117, doi:10.1029/91PA02994, 1992.

Hyun, S., Ahagon, N., and Yoon, H.: Milankovitch cycles and paleoceanographic evolution within sediments from ODP Sites 980 and 983 of the North Atlantic Ocean, Geosciences journal, 9, 235–242, doi:10.1007/BF02910583, 2005.

Iglesias-Rodriguez, M. D., Halloran, P. R., Rickaby, R. E. M., Hall, I. R., Colmenero-Hidalgo, E., Gittins, J. R., Green, D. R. H., Tyrrell, T., Gibbs, S. J., von Dassow, P., Rehm, E., Armbrust, E. V., and Boessenkool, K. P.: Phytoplankton calcification in a high-CO2 world., Science, 320, 336–40, doi:10.1126/science.1154122, 2008.

Imbrie, J., McIntyre, A., and Mix, A.: Oceanic response to orbital forcing in the late Quaternary: observational and experimental strategies, pp. 121–164, Kluwer Academic, Boston, a. Berger, S.H. Schneider, and J.-C. Duplessy (Eds.), 1989.

Ingle, S.: Solubility of calcite in the ocean, Marine chemistry, 3, 301–319, doi:10.1016/0304-4203(75)90010-9, 1975.

Joos, F., Roth, R., Fuglestvedt, J., Peters, G., Enting, I., von Bloh, W., Brovkin, V., Burke, E., Eby, M., NR, Friedrich, T., Frölicher, T., Halloran, P., Holden, P., Jones, C., Kleinen, T., Mackenzie, F., Matsumoto, K., Meinshausen, M., Plattner, G., Reisinger, A., Segschneider, J., Shaffer, G., Steinacher, M., Strassmann, K., Tanaka, K., Timmermann, A., and Weaver, A.: Carbon dioxide and climate impulse response functions for the computation of greenhouse gas metrics: a multi-model analysis, Atmospheric chemistry and physics, 13, 2793–2825, doi:10.5194/acp-13-2793-2013, 2013.

Jouzel, J.: EPICA Dome C Ice Cores Deuterium Data, IGBP PAGES, World Data Center for Paleoclimatology, Data Contribution Series no. 2004 - 038. NOAA/NGDC Paleoclimatology Program, Boulder CO, USA, doi:10.3334/CDIAC/cli.007, 2004.

Jouzel, J., Lorius, C., Petit, J., Genthon, C., Barkov, N., Kotlyakov, V., and Petrov, V.: Vostok ice core - a continuous isotope temperature record over the last climatic cycle (160,000 years), Nature, 329, 403–408, doi:10.1038/329403a0, 1987.

Jung, S. and Sarnthein, M.: Stable isotope data of sediment cores GIK23415-9, data set, PANGAEA, doi:10.1549/PANGAEA.112912, 2003a.

Jung, S. and Sarnthein, M.: Stable isotope data of sediment cores GIK23418-9, data set, PANGAEA, doi:10.1549/PANGAEA.112915, 2003b.

Jung, S. and Sarnthein, M.: Stable isotope data of sediment cores GIK23414-9, data set, PANGAEA, doi:10.1549/PANGAEA.112911, 2003c.

Jung, S. and Sarnthein, M.: Stable isotope data of sediment cores GIK23415-9, data set, PANGAEA, doi:10.1549/PANGAEA.112912, 2003d.

Jung, S. and Sarnthein, M.: Stable isotope analysis of foraminifera from sediment cores GIK17049-6, data set, PANGAEA, doi:10.1549/PANGAEA.112908, 2004.

Kawahata, H., Suzuki, A., and Ahagon, N.: Biogenic sediments in the West Caroline Basin, the western equatorial Pacific during the last 330,000 years, Marine geology, 149, 155–176, doi:10.1016/S0025-3227(98)00039-5, 1998.

Kawahata, H., Okamoto, T., and Ujiie, E. M. H.: Fluctuations of eolian flux and ocean productivity in the mid-latitude North Pacific during the last 200 kyr, Quaternary science reviews, 19, 1279–1291, doi:10.1016/S0277-3791(99)00096-7, 2000.

Kawamura, H., Holbourn, A., and Kuhnt, W.: Climate variability and land-ocean interactions in the Indo Pacific Warm Pool: A 460-ka palynological and organic geochemical record from the Timor Sea, Marine micropaleontology, 59, 1–14, doi:10.1016/j.marmicro.2005.09.001, 2006.

Keigwin, L.: Radiocarbon and stable isotope constraints on Last Glacial Maximum and Younger Dryas ventilation in the western North Atlantic, Paleoceanography, 19, doi:10.1029/2004PA001029, 2004.

Kirst, G.: Rekonstruktion von Oberflächenwassertemperaturen im östlichen Südatlantik anhand von Alkenonen, Berichte, Fachbereich Geowissenschaften, Universität Bremen, 118, 130 pp, 1998.

Kirst, G., Schneider, R., Müller, P., Von Storch, I., and Wefer, G.: Late Quaternary temperature variability in the Benguela Current System derived from alkenones, Quaternary research, 52, 92–103, doi:10.1006/qres.1999.2040, 1999.

Kuhn, G.: Calcium carbonate content of sediment core PS2489-2, Alfred Wegener Institute for Polar and Marine Research, Bremerhaven, data set, PANGAEA, doi:doi:10.1594/PANGAEA.56102, 1999.

LaMontagne, R., Murray, R., Wei, K., Leinen, M., and Wang, C.: Decoupling of carbonate preservation, carbonate concentration, and biogenic accumulation: A 400-kyr record from the central equatorial Pacific Ocean, Paleoceanography, 11, 553–562, doi:10.1029/96PA02249, 1996.

Lanczos, C.: Linear differential operators, D. Van Nostrand Company Ltd., London et al., 564 p., 1961.

5   Le Quéré, C., Peters, G., Andres, R., Andrew, R., Boden, T., Ciais, P., Friedlingstein, P., Houghton, R., Marland, G., Moriarty, R., Sitch, S., Tans, P., Arneth, A., Arvanitis, A., Bakker, D., Bopp, L., Canadell, J., Chini, L., Doney, S., Harper, A., Harris, I., House, J., Jain, A., Jones, S., Kato, E., Keeling, R., Goldewijk, K., Körtzinger, A., Koven, C., Lefèvre, N., Maignan, F., Omar, A., Ono, T., Park, G., Pfeil, B., Poulter, B., Raupach, M., Regnier, P., Roedenbeck, C., Saito, S., Schwinger, J., Segschneider, J., Stocker, B., Takahashi, T., Tilbrook, B., van Heuven, S., Viovy, N., Wanninkhof, R., Wiltshire, A., and Zaehle, S.: Global carbon budget 2013, Earth system science data, 6, 10   235–263, doi:10.5194/essd-6-235-2014, 2014.

Lean, C. and McCave, I.: Glacial to interglacial mineral magnetic and palaeoceanographic changes at Chatham Rise, SW Pacific Ocean, Earth and planetary science letters, 163, 247–260, doi:10.1016/S0012-821X(98)00191-5, 1998.

Li, Y. and Gregory, S.: Diffusion of ions in sea water and deep sea sediments, Geochimica et cosmochimica acta, 38, 703–714, doi:10.1016/0016-7037(74)90145-8, 1974.

15   Little, M., Schneider, R., Kroon, D., Bickert, T., and Wefer, G.: Rapid palaeoceanographic changes in the Benguela Upwelling System for the last 160,000 years as indicated by abundances of planktonic foraminifera, Palaeogeography, Palaeoclimatology, Palaeoecology, 130, 135–161, doi:10.1016/S0031-0182(96)00136-8, 1997.

Lyle, M., Mix, A., and Pisias, N.: Patterns of $CaCO_3$ deposition in the eastern tropical Pacific Ocean for the last 150 kyr: Evidence for a southeast Pacific depositional spike during marine isotope stage (MIS) 2, Paleoceanography, 17, doi:10.1029/2000PA000538, 2002.

20   Mackensen, A. and Bickert, T.: Stable Carbon Isotopes in Benthic Foraminifera: Proxies for Deep and Bottom water Circulation and New Production, pp. 229–254, Springer, Berlin, Heidelberg, g. Fischer and G. Wefer (Eds.), 1999.

Mackensen, A., Grobe, H., Hubberten, H., and Kuhn, G.: Benthic foraminiferal assemblages and the δ^{13}C-signal in the Atlantic sector of the Southern Ocean: glacial-to-interglacial contrasts, pp. 105–144, Springer-Verlag, Berlin, Heidelberg, r. Zahn, T.F. Pederson, M.A. Kaminiski, and L. Labeyrie (Eds.), 1994.

25   Maeda, L., Kawahata, H., and Nohara, M.: Fluctuation of biogenic and abiogenic sedimentation on the Shatsky Rise in the western North Pacific during the late Quaternary, Marine geology, 189, 197–214, doi:10.1016/S0025-3227(02)00405-X, 2002.

Mahowald, N., Kohfeld, K., hansson, M., Balkanski, Y., Harrison, S., Prentice, I., Schulz, M., and Rodhe, H.: Dust sources and deposition during the last glacial maximum and current climate: A comparison of model results with paleodata from ice cores and marine sediments, Journal of Geophysical Research: Atmospheres, 104, 15 895–15 916, doi:10.1029/1999JD900084, 1999.

30   Maier-Reimer, E.: Geochemical cycles in an ocean general circulation model - preindustrial tracer distributions, Global biogeochemical cycles, 7, 645–677, doi:10.1029/93GB01355, 1993.

Maier-Reimer, E. and Hasselmann, K.: Transport and storage of CO_2 in the ocean - an inorganic ocean-circulation carbon cycle model, Climate dynamics, 2, 63–90, doi:10.1007/BF01054491, 1987.

Maier-Reimer, E., Mikolajewicz, U., and Hasselmann, K.: Mean circulation of the Hamburg LSG OGCM and its sensitivity to the thermo-35   haline surface forcing, Journal of Physical Oceanography, 23, 731–757, doi:10.1175/1520-0485(1993)023<0731:MCOTHL>2.0.CO;2, 1993.

Maier-Reimer, E., Kriest, I., Segschneider, J., and Wetzel, P.: The HAMburg Ocean Carbon Cycle Model HAMOCC 5.1 - Technical Description Release 1.1 -, Tech. rep., Max Planck Institute for Meteorology, Hamburg, Germany, Series: Berichte zur Erdsystemforschung, no. 14, ISSN 1614-1199, 2005.

MARGO Project Members: Constraints on the magnitude and patterns of ocean cooling at the Last Glacial Maximum, Nature geoscience, 2,
5   127–132, doi:10.1038/NGEO412, 2009.

Martin, B.: Statistics for physicists, Academic Press, London and New York, 209 p., 1971.

Martin, J., Coale, K., Johnson, K., Gordon, S. F. R., Tanner, S., Hunter, C., ELROD, V., Coley, J. N. T., Barber, R., Lindley, S., Watson, A., Vanscoy, K., Law, C., Liddicoat, M., Ling, R., Stanton, T., Stockel, J., Collins, C., Anderson, A., Bidigare, R., Ondrusek, M., Latasa, M., Millero, F., Lee, K., Yao, W., Zhang, J., Friedrich, G., Sakamoto, C., Chavez, F., Buck, K., Kolber, Z., Greene, R., Falkowski, P.,
10   Chisholm, S., Hoge, F., Swift, R., Yungel, J., Turner, S., Nightingale, P., Hatton, A., Liss, P., and Tindale, N.: Testing the iron hypothesis in ecosystems of the equatorial Pacific Ocean, Nature, 371, 123–129, doi:10.1038/371123a0, 1994.

Martinson, D., Pisias, N., Hays, J., Imbrie, J., Moore, T., and Shackleton, N.: Age Dating and the orbital theory of the ice ages: development of a high-resolution 0 to 300,000-year chronostratigraphy, Quaternary research, 27, 1–29, doi:10.1016/0033-5894(87)90046-9, 1987.

Matsu'ura, M. and Hirata, N.: Generalized least-squares solution to quasi-linear inverse problems with a priori information, Journal of
15   Physics of the Earth,, 30, 451–468, doi:10.1029/RG010i001p00251, 1982.

McCave, I., Carter, L., and Hall, I.: Glacial-interglacial changes in water mass structure and flow in the SW Pacific Ocean, Quaternary science reviews, 27, 1886–1908, doi:10.1016/j.quascirev.2008.07.010, 2008.

McIntyre, A.: Surface water response of the equatorial Atlantic Ocean to orbital forcing, Paleoceanography, 4, 19–55, doi:10.1029/PA004i001p00019, 1989.

20   McIntyre, A. and Imbrie, J.: Stable isotopes of sediment core V30-97 (specmap.011), data set, PANGAEA, doi:10.1594/PANGAEA.56356, 2000.

Mehrbach, C., Culberson, C., Hawley, J., and Pytkowic, R.: Measurement of apparent dissociation constants of carbonic acid in seawater at atmospheric pressure, Limnology and oceanography, 18, 897–907, doi:10.4319/lo.1973.18.6.0897, 1973.

Mix, A. C.: Carbon 13 in Pacific deep and intermediate waters, 0-370 KA: Implications for ocean circulation and Pleistocene CO_2, Paleo-
25   ceanography, 6, 205–226, doi:10.1029/90PA02303, 1991.

Mollenhauer, G., Schneider, R., Müller, P., Spiess, V., and Wefer, G.: Glacial/interglacial variability in the Benguela upwelling system: Spatial distribution and budgets of organic carbon accumulation, Global biogeochemical cycles, 16, doi:10.1029/2001GB001488, 2002.

Moy, A., Howard, W., and Gagan, M.: Late Quaternary palaeoceanography of the Circumpolar Deep Water from the South Tasman Rise, JQS. Journal of quaternary science, 21, 763–777, doi:10.1002/jqs.1067, 2006.

30   Müller, P.: Carbon and nitrogen data of sediment core GeoB1711-4, data set, PANGAEA, doi:doi:10.1594/PANGAEA.143593, 2006.

Murray, R., Knowlton, C., Leinen, M., Mix, A., and Polsky, C.: Export production and carbonate dissolution in the central equatorial Pacific Ocean over the past 1 Myr, Paleoceanography, 15, 570–592, doi:10.1029/1999PA000457, 2000.

Neftel, A., Oeschger, H., Schwander, J., Stauffer, B., and Zumbrunn, R.: Ice core sample measurements give atmospheric CO_2 content during the past 40,000 YR, Nature, 295, 220–223, doi:10.1038/295220a0, 1982.

35   Ninkovich, D. and Shackleton, N.: Distribution, stratigraphic position and age of ash layer-L, in Panama Basin region, Earth and Planetary Science Letters, 27, 20–34, doi:10.1016/0012-821X(75)90156-9, 1975.

O'ishi, R. and Abe-Ouchi, A.: Influence of dynamic vegetation on climate change and terrestrial carbon storage in the Last Glacial Maximum, Climate of the past, 9, 1571–1587, doi:10.5194/cp-9-1571-2013, 2013.

Oliver, K., Hoogakker, B., Crowhurst, S., Henderson, G., Rickaby, R., Edwards, N., and Elderfield, H.: A synthesis of marine sediment core δ^{13}C data over the last 150 000 years, Climate of the past, 6, 645–673, doi:10.5194/cp-6-645-2010, 2010.

Parsons, T. and Takahashi, M.: Biological oceanographic processes, Pergamon Press, Oxford et al., 166 p., 1973.

Pierre, C., Saliege, J., Urrutiaguer, M., and Giraudeau, J.: Stable isotope record of the last 500 k.y. at Site 1087 (Southern Cape Basin), Proc. Ocean Drill. Program Sci. Results, 19, 22 p., 2004.

Pisias, N. and Mix, A.: Spatial and temporal oceanographic variability of the eastern equatorial Pacific during the late Pleistocene: Evidence from Radiolaria microfossils, Paleoceanography, 12, 381–393, doi:10.1029/97PA00583, 1997.

Ragueneau, O., Treguer, P., Leynaert, A., Anderson, R., Brzezinski, M., DeMaster, D., Dugdale, R., Dymond, J., Fischer, G., Francois, R., Heinze, C., Maier-Reimer, E., Martin-Jézéquel, V., Nelson, D., and Quéguiner, B.: A review of the Si cycle in the modem ocean: recent progress and missing gaps in the application of biogenic opal as a paleoproductivity proxy, Global and planetary change, 26, 317–365, doi:10.1016/S0921-8181(00)00052-7, 2000.

Rau, A., Rogers, J., Lutjeharms, J., Giraudeau, J., Lee-Thorp, J., M.-T. Chen, and Waelbroeck, C.: A 450-kyr record of hydrological conditions on the western Agulhas Bank Slope, south of Africa, Marine geology, 180, 183–201, doi:10.1016/S0025-3227(01)00213-4, 2002.

Raven, J.: Ocean acidification due to increasing atmospheric carbon dioxide, The Royal Society (Science Policy Section), London, 60 p., 2005.

Rea, D., Chambers, L., Chuey, J., Janacek, T., Leinen, M., and Pisias, N.: A 420,000-year record of cyclicity in oceanic and atmospheric processes from the eastern equatorial Pacific, Paleoceanography, 1, 577–586, doi:10.1029/PA001i004p00577, 1986.

Retallack, G. J.: Methane release from igneous intrusion of coal during late permian extinction events, The journal of geology, 116, 1–20, doi:10.1086/524120, http://tinyurl.sfx.mpg.de/u7dw, 2008.

Riebesell, U., Zondervan, I., Rost, B., Tortell, P. D., Zeebe, R. E., and Morel, F. M.: Reduced calcification of marine plankton in response to increased atmospheric CO_2, Nature, 407, 364–7, doi:10.1038/35030078, http://tinyurl.sfx.mpg.de/u77b, 2000.

Riebesell, U., Schulz, K., Bellerby, R., Botros, M., Fritsche, P., Meyerhöfer, M., Neill, C., Nondal, G., Oschlies, A., Wohlers, J., and Zöllner, E.: Enhanced biological carbon consumption in a high CO_2 ocean, Nature, 450, 545–8, doi:10.1038/nature06267, 2007.

Ruddiman, W. and Farrell, J.: Calcium carbonate content of sediment core RC13-228, data set, PANGAEA, doi:doi:10.1594/PANGAEA.51105, 1996a.

Ruddiman, W. and Farrell, J.: Calcium carbonate content of sediment core V25-59, data set, PANGAEA, doi:10.1594/PANGAEA.51257, 1996b.

Ruddiman, W., Raymo, M., Martinson, D., Clement, B., and Backman, J.: Pleistocene evolution: northern hemisphere ice sheets and North Atlantic Ocean, Paleoceanography, 4, 353–412, doi:10.1029/PA004i004p00353, 1989.

Sarnthein, M., Erlenkeuser, H., Grafenstein, R. V., and Schröder, C.: Stable-isotope stratigraphy for the last 750,000 years:"Meteor" core 13519 from the eastern equatorial Atlantic, Meteor Forschungsergeb., Reihe C, 38, 9–24, 1984.

Sarnthein, M., Winn, K., Jung, S., Duplessy, J., Labeyrei, L., Erlenkeuser, H., and Ganssen, G.: Changes in east Atlantic deep-water circulation over the last 30,000 years - 8 time slice reconstructions, Paleoceanography, 9, 209–267, doi:10.1029/93PA03301, 1994.

Schlünz, B.: Riverine Organic Carbon Input into the Ocean in Relation to Late Quaternary Climate Change, Berichte, Fachbereich Geowissenschaften, Universität Bremen, 116, 136 pp., 1998.

Schlünz, B., Schneider, R., Müller, P., and Wefer, G.: (Table 2) Total organic and inorganic carbon contents, and stable carbon isotope ratios of sediment core GeoB3935-2, data set, PANGAEA, doi:dx.doi.org/10.1594/PANGAEA.54943, 2000.

Schlunz, B., Schneider, R., Müller, P., and Wefer, G.: Late Quaternary organic carbon accumulation south of Barbados: influence of the Orinoco and Amazon rivers?, Deep-sea research. Part 1. Oceanographic research papers, 47, 1101–1124, doi:10.1016/S0967-0637(99)00076-X, 2000.

Schmiedl, G. and Mackensen, A.: Late quaternary paleoproductivity and deep water circulation in the eastern South Atlantic Ocean: Evidence
5   from benthic foraminifera, Palaeogeography, Palaeoclimatology, Palaeoecology, 130, 43–80, doi:10.1016/S0031-0182(96)00137-X, 1997.

Schmiedl, G. and Mackensen, A.: Stable oxygen isotope records of different benthic foraminiferal species of core GeoB3004-1 from the western Arabian Sea, data set, PANGAEA, doi:10.1594/PANGAEA.548185, 2006.

Shackleton, N.: Carbon-13 in Uvigerina: Tropical rain forest history and the equatorial Pacific carbonate dissolution cycles, pp. 401–428, Plenum, New York, nR Andersen and A Malahoff (Eds.), 1977.

10 Shackleton, N. and Pisias, N.: Atmospheric carbon dioxide, orbital forcing, and climate, pp. 303–317, American Geophysical Union, Washington, D.C., E.T. Sundquist and W.S. Broecker (Eds.), Geophysical Monograph 32, 1985.

Shakun, J. D., Clark, P. U., He, F., Marcott, S. A., Mix, A. C., Liu, Z., Otto-Bliesner, B., Schmittner, A., and Bard, E.: Global warming preceded by increasing carbon dioxide concentrations during the last deglaciation., Nature, 484, 49–54, doi:10.1038/nature10915, 2012.

Siegenthaler, U., Stocker, T. F., Monnin, E., Lüthi, D., Schwander, J., Stauffer, B., Raynaud, D., Barnola, J.-M., Fischer, H.,
15 Masson-Delmotte, V., and Jouzel, J.: Stable carbon cycle-climate relationship during the Late Pleistocene., Science, 310, 1313–7, doi:10.1126/science.1120130, 2005.

Sigman, D. and Boyle, E.: Glacial/interglacial variations in atmospheric carbon dioxide, Nature, 407, 859–69, doi:10.1038/35038000, 2000.

Smith, C. and Rabouille, C.: What controls the mixed-layer depth in deep-sea sediments? The importance of POC flux, Limnology and oceanography, 47, 418–426, doi:10.4319/lo.2002.47.2.0418, 2002.

20 Stute, M., Forster, M., Frischkorn, H., Serejo, A., Clark, J., Schlosser, P., Broecker, W., and Bonani, G.: Cooling of tropical Brazil (5degC) during the last glacial maximum, Science, 269, 379–383, doi:10.1126/science.269.5222.379, 1995.

Svensen, H., Planke, S., Polozov, A., Schmidbauer, N., Corfu, F., Podladchikov, Y., and Jamtveit, B.: Siberian gas venting and the end-Permian environmental crisis, Earth and planetary science letters, 277, 490–500, doi:10.1016/j.epsl.2008.11.015, 2009.

Thomson, J., Nixon, S., Summerhayes, C., Schönfeld, J., Zahn, R., and Grootes, P.: Implications for sedimentation changes on the Iberian
25 margin over the last two glacial/interglacial transitions from (Th-230(excess))(0) systematics, Earth and planetary science letters, 165, 255–270, doi:10.1016/S0012-821X(98)00265-9, 1999.

Thomson, J., Nixon, S., Summerhayes, C., Rohling, E., Schönfeld, J., Zahn, R., Grootes, P., Abrantes, F., Gaspar, L., and Vaqueiro, S.: Enhanced productivity on the Iberian margin during glacial/interglacial transitions revealed by barium and diatoms, Journal of the Geological Society, 157, 667–677, doi:10.1144/jgs.157.3.667, 2000.

30 Turley, C. and Mackie, P.: Bacterial and cyanobacterial flux to the deep NE Atlantic on sedimenting particles, Deep-sea research. Part 1. Oceanographic research papers, 42, 1453–1474, doi:10.1016/0967-0637(95)00056-C, 1995.

Ullman, W. and Aller, R.: Diffusion coefficients in nearshore marine sediments, Limnology and Oceanography, 27, 552–556, doi:10.4319/lo.1982.27.3.0552, 1982.

Van Cappellen, P., Dixit, S., and van Beusekom, J.: Biogenic silica dissolution in the oceans: Reconciling experimental and field-based
35 dissolution rates, Global biogeochemical cycles, 16, doi:10.1029/2001GB001431, 2002.

Verardo, D. and McIntyre, A.: Production and destruction: Control of biogenous sedimentation in the tropical Atlantic 0-300,000 Years B.P., Paleoceanography, 9, 63–86, doi:10.1029/93PA02901, 1994.

Weiss, R.: The solubility of nitrogen, oxygen and argon in water and seawater, Deep-sea research and oceanographic abstracts, 17, 721–735, doi:10.1016/0011-7471(70)90037-9, 1970.

Weiss, R.: Carbon dioxide in water and seawater: The solubility of a non-ideal gas, Marine Chemistry, 2, 203–215, 1974.

Weyhenmeyer, C., Burns, S., Waber, H., Aeschbach-Hertig, W., Kipfer, R., Loosli, H., and Matter, A.: Cool glacial temperatures and changes in moisture source recorded in Oman groundwaters, Science, 287, 842–845, doi:10.1126/science.287.5454.842, 2000.

Wiggins, R.: The general linear inverse problem: Implication of surface waves and free oscillations for Earth structure, Reviews of geophysics, 10, 251–285, doi:10.1029/RG010i001p00251, 1972.

Winguth, A., Archer, D., Duplessy, J., Maier-Reimer, E., and Mikolajewicz, U.: Sensitivity of paleonutrient tracer distributions and deep-sea circulation to glacial boundary conditions, Paleoceanography, 14, 304–323, doi:10.1029/1999PA900002, 1999.

Wunsch, C.: Tracer inverse problems, pp. 1–77, Kluwer Academic Publishers, Dordrecht, DLT Anderson and J Willebrand (Eds.), 1989.

Yu, J., Anderson, R., and Rohling, E.: Deep Ocean Carbonate Chemistry and Glacial-Interglacial Atmospheric CO2 Changes, Oceanography, 27, 16–25, doi:10.5670/oceanog.2014.04, 2014.

Zabel, M., Bickert, T., and Dittert, L.: Significance of the sedimentary Al : Ti ratio as an indicator for variations in the circulation patterns of the equatorial North Atlantic, Paleoceanography, 14, 789–799, doi:10.1029/1999PA900027, 1999.

Zachos, J. C., Röhl, U., Schellenberg, S. A., Sluijs, A., Hodell, D. A., Kelly, D. C., Thomas, E., Nicolo, M., Raffi, I., Lourens, L. J., McCarren, H., and Kroon, D.: Rapid acidification of the ocean during the Paleocene-Eocene thermal maximum., Science, 308, 1611–5, doi:10.1126/science.1109004, 2005.

Zahn, R., Wynn, K., and Sarnthein, M.: Benthic foraminiferal δ^{13}C and accumulation rates of organic carbon: Uvigerina Peregrina group and Cibicidoides Wuellerstorfi, Paleoceanography, 1, 27–42, doi:10.1029/PA001i001p00027, 1986.

Zahn, R., Schönfeld, J., Kudrass, H., Park, M., H Erlenkeuser, H., and Grootes, P.: Thermohaline instability in the North Atlantic during meltwater events: Stable isotope and ice-rafted detritus records from core SO75-26KL, Portuguese margin, Paleoceanography, 12, 696–710, doi:10.1029/97PA00581, 1997.

Zeng, N.: Glacial-interglacial atmospheric CO_2 change - The glacial burial hypothesis, Advances in Atmospheric Sciences, 20, 677–693, doi:10.1007/BF02915395, 2003.

Zondervan, I., Zeebe, R., Rost, B., and Riebesell, U.: Decreasing marine biogenic calcification: A negative feedback on rising atmospheric pCO(2), Global biogeochemical cycles, 15, 507–516, doi:10.1029/2000GB001321, 2001.
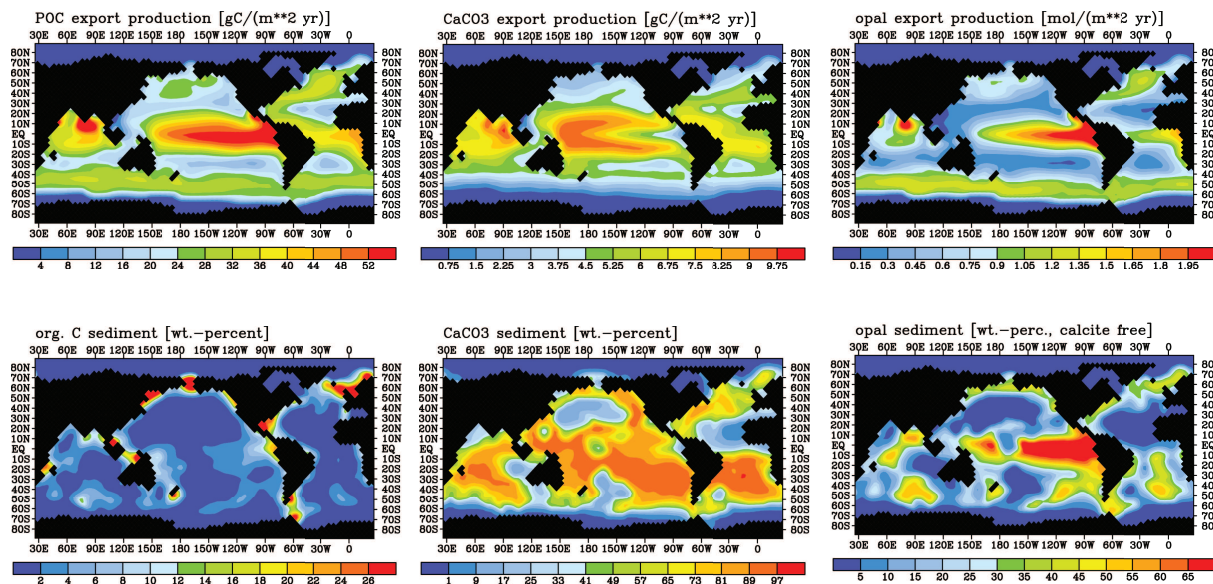
Figure 1. Export production rates and average surface sediment distributions for the control run.
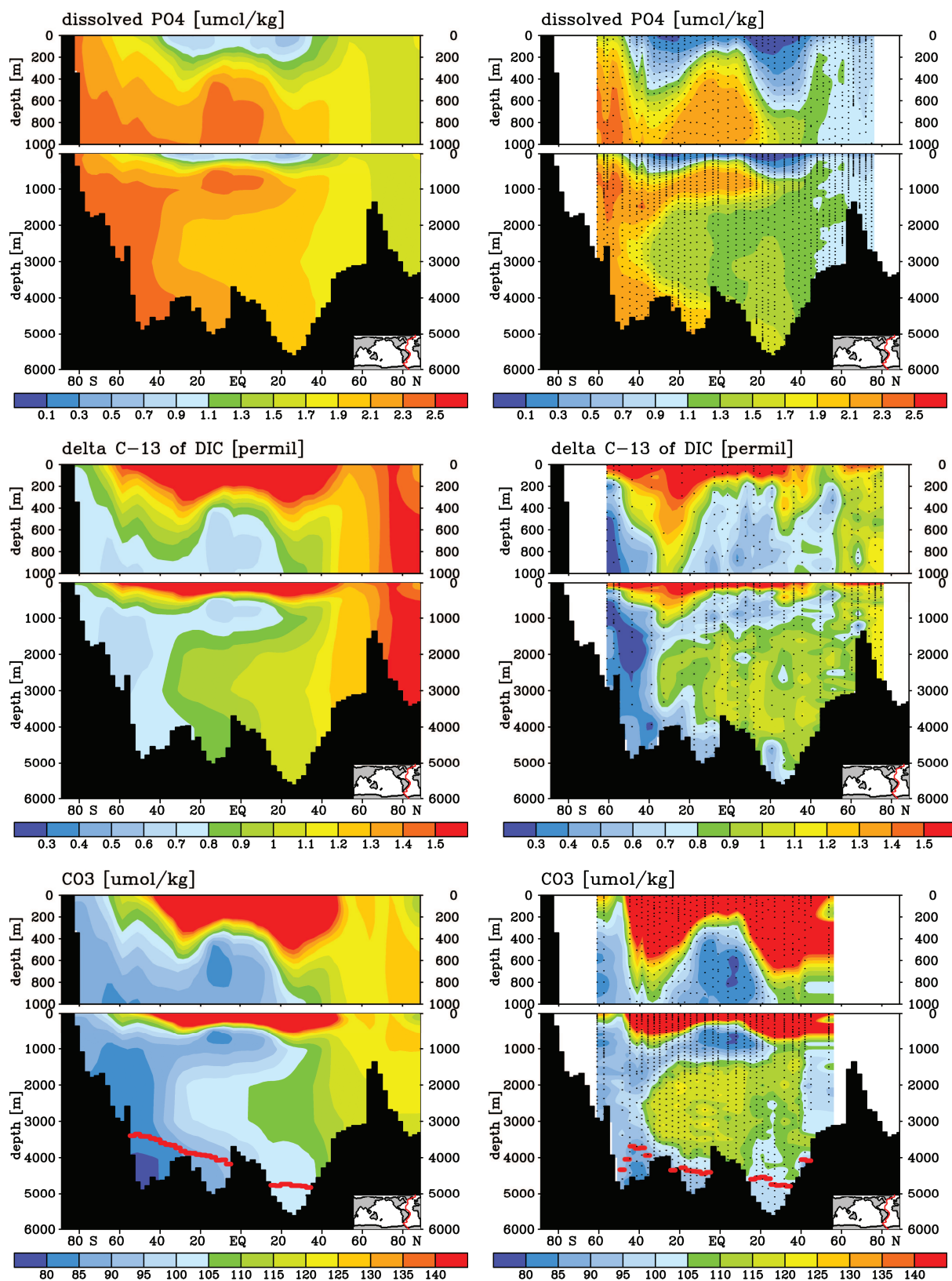
Figure 2. Atlantic Ocean cross sections for the model control run (left column) and observations from the GEOSECS programme (right column). Top: Dissolved phosphate. Centre: $\delta^{13}C$ of total dissolved inorganic carbon. Bottom: Carbonate ion concentration.
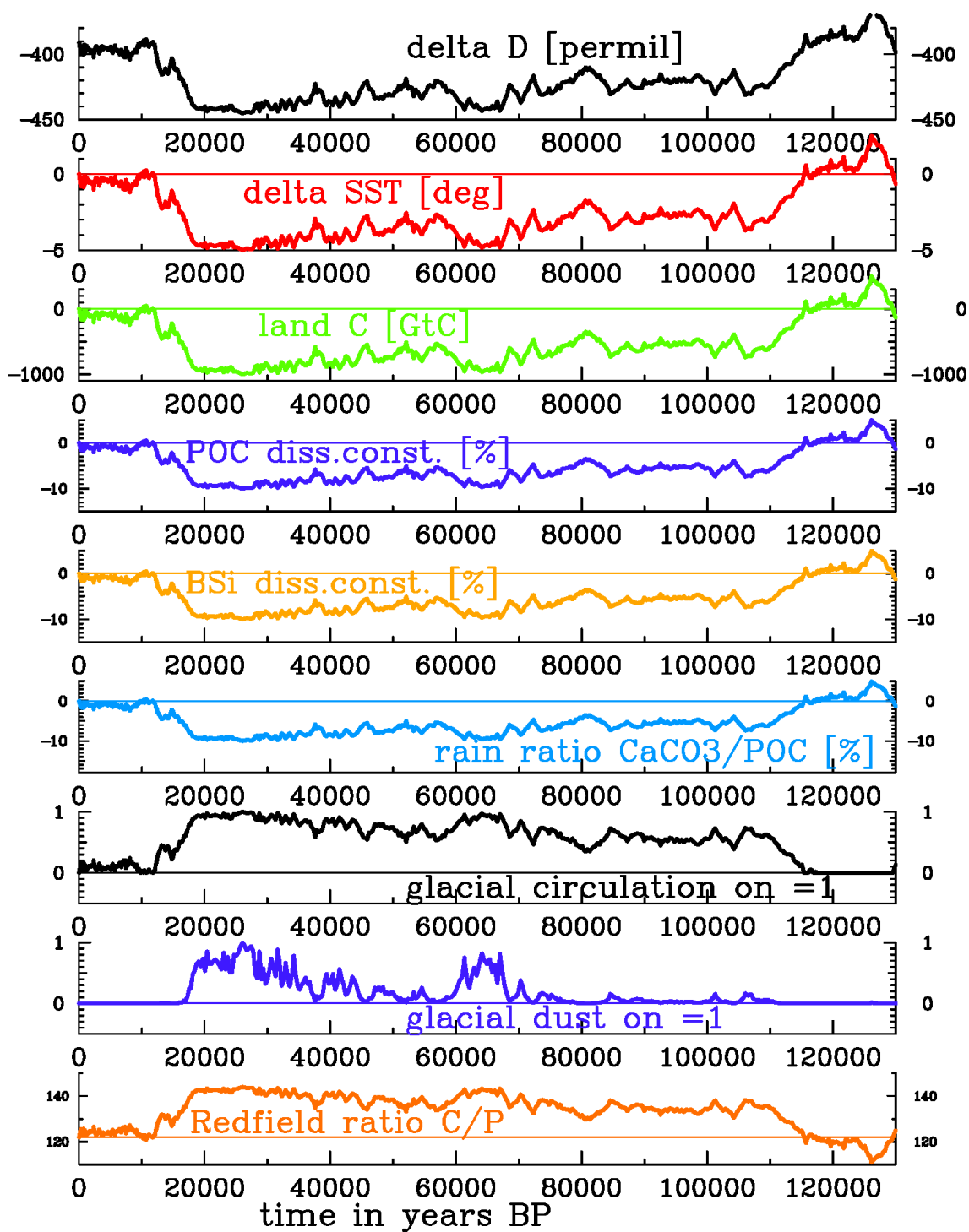
Figure 3. Prescribed parameter changes for the sensitivity experiemnts with the biogeochemcial ocean model.
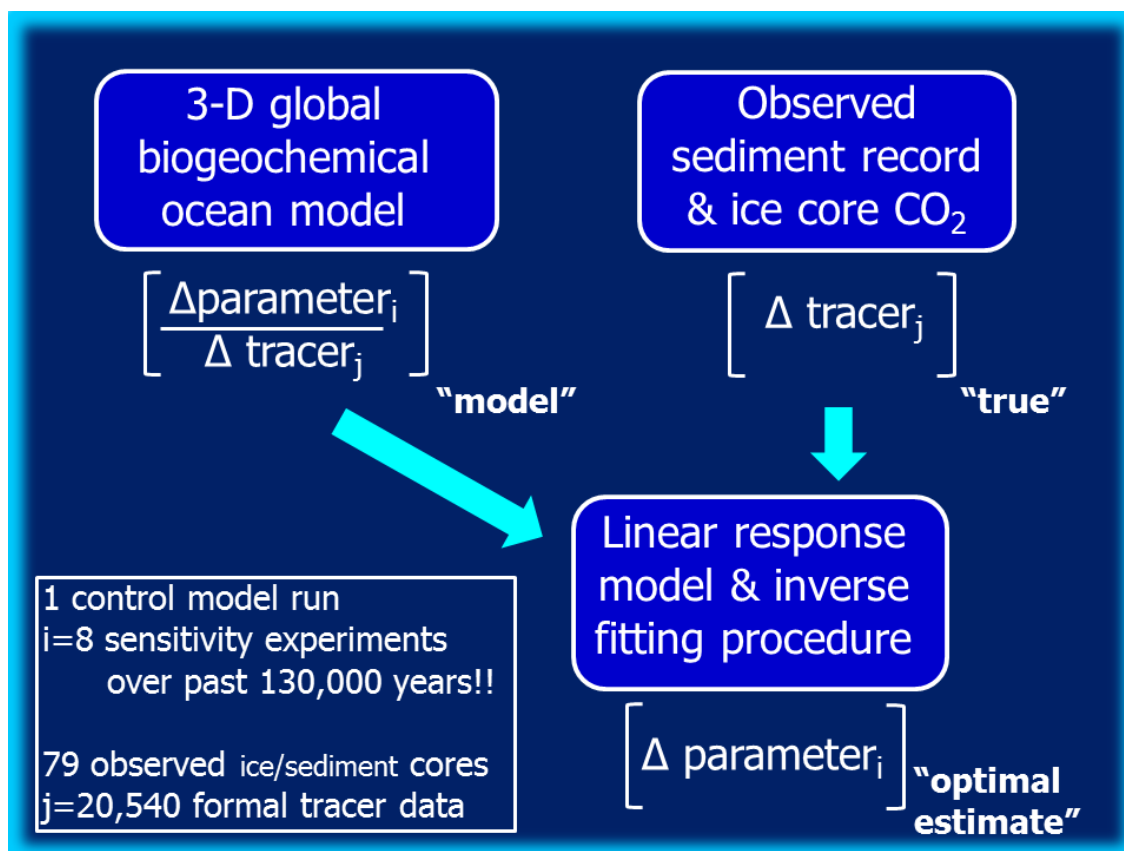
Figure 4. Fitting procedure combining the observed paleo-climate data and the model derived information on how the downcore distributions of the various cores look like for the different sensitivity experiments.
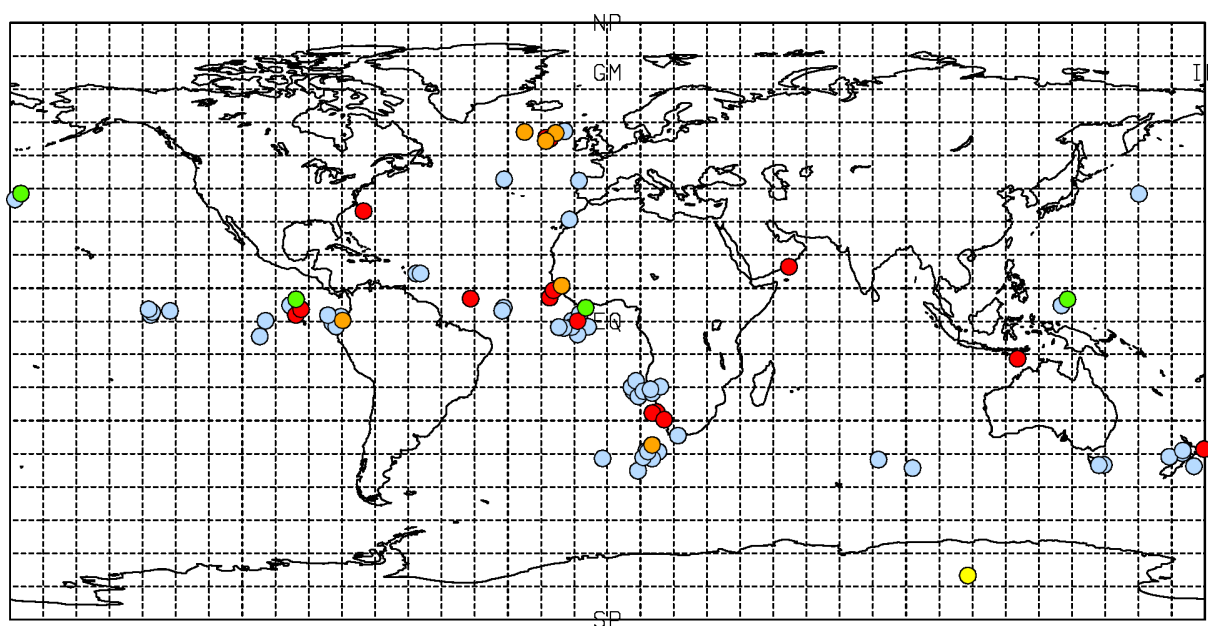
Figure 5. Locations of the paleo-climate observations (sediment core, ice core) as used in the inverse approach: atmospheric CO_2 (yellow), $\delta^{13}C_{benthic}$ (red), $\delta^{13}C_{planktonic}$ (orange), BSi wt-% (green), and $CaCO_3$ wt-% (blue).
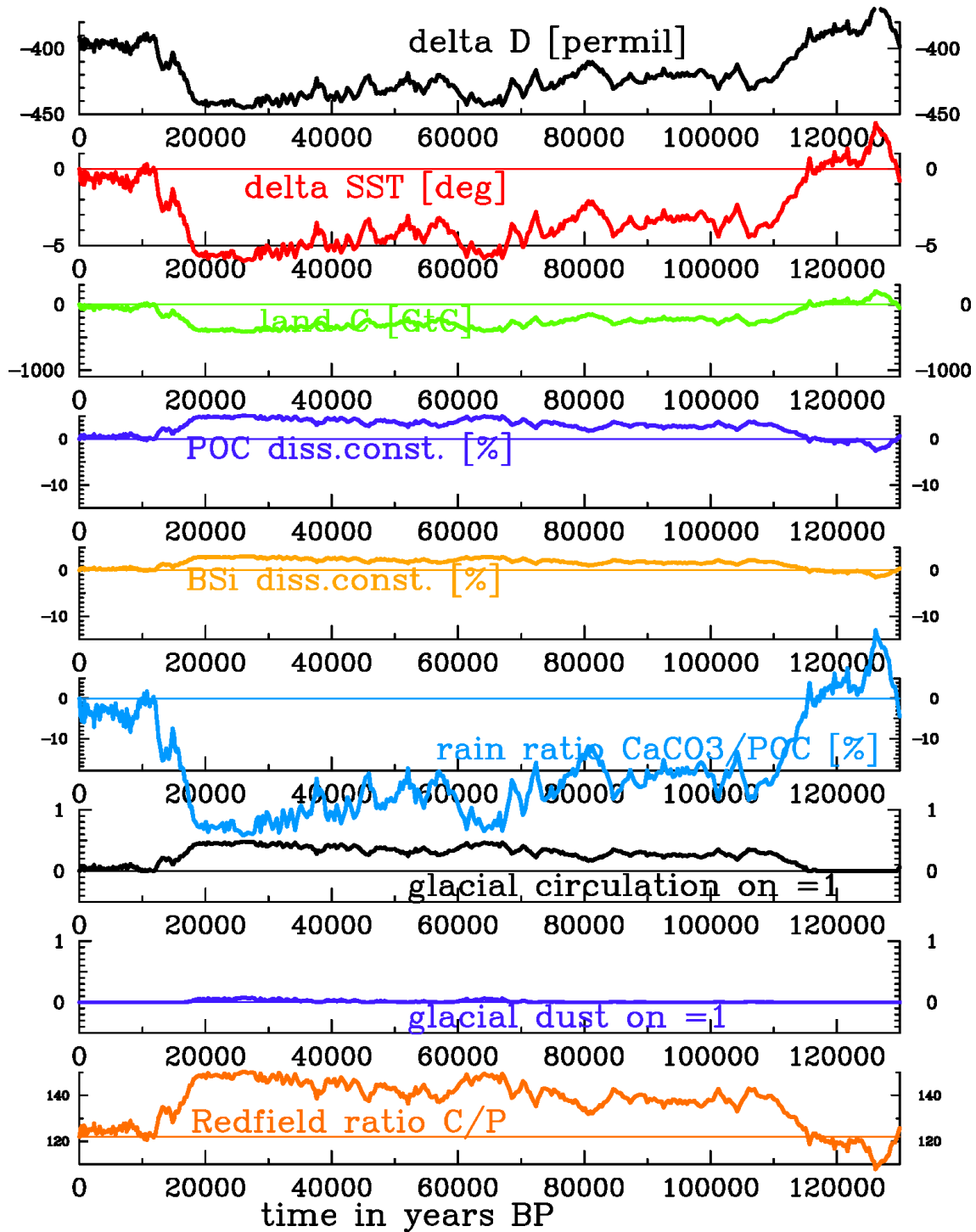
Figure 6. Resulting parameter variations of the past climatic cycle for the full rank solution of the linear response model.
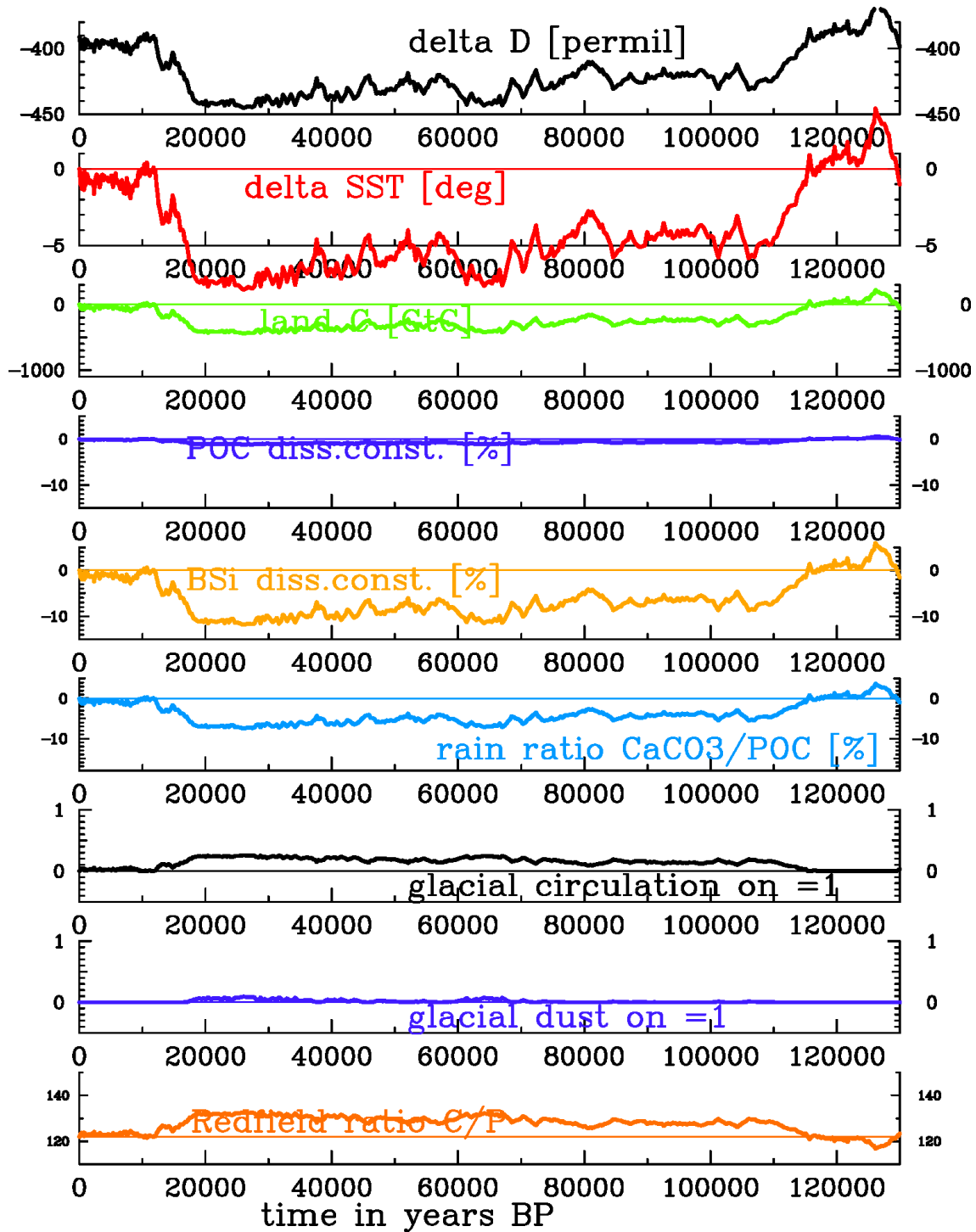
Figure 7. Resulting parameter variations of the past climatic cycle for the rank 7 solution of the linear response model.
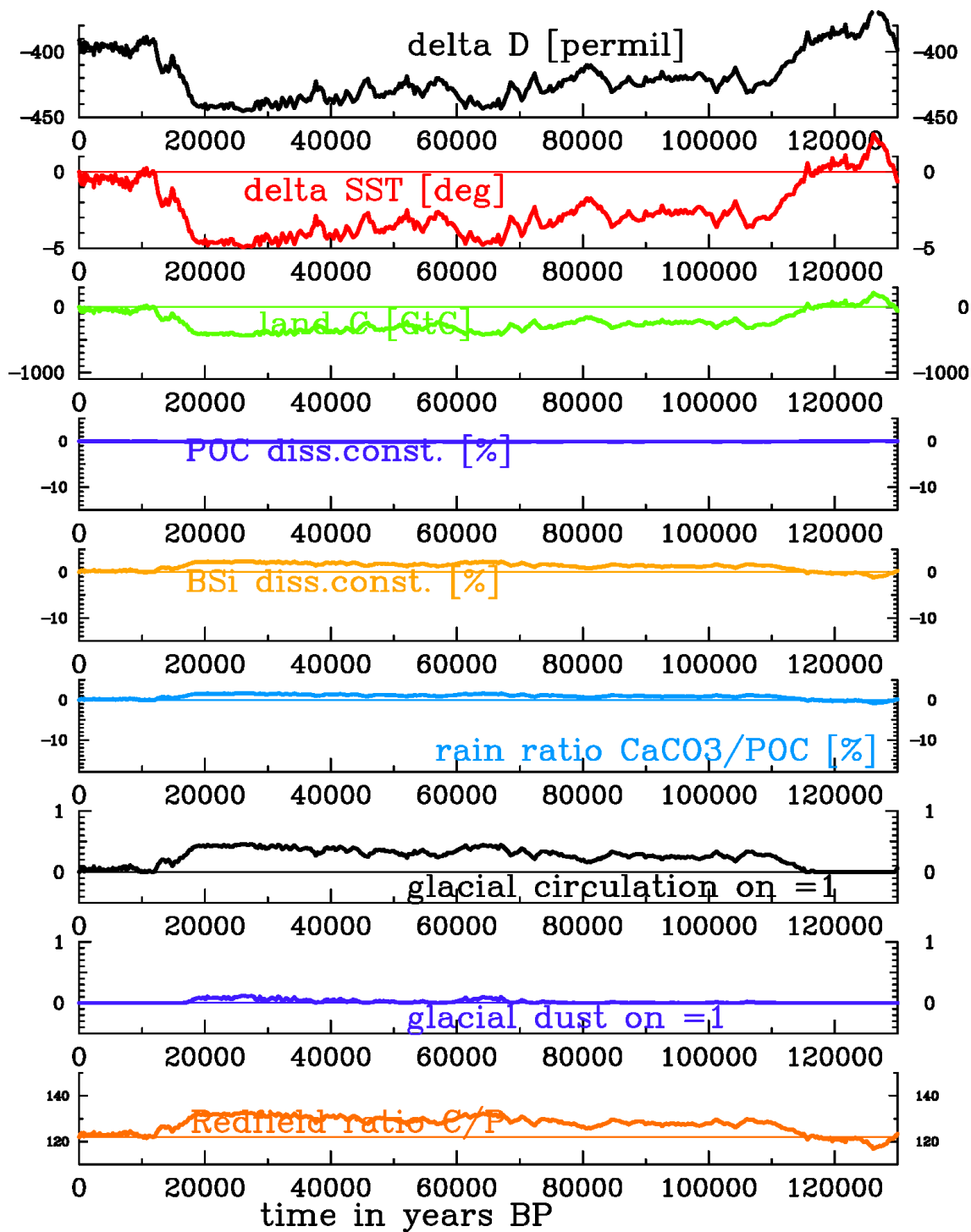
Figure 8. Resulting parameter variations of the past climatic cycle for the rank 6 solution of the linear response model.
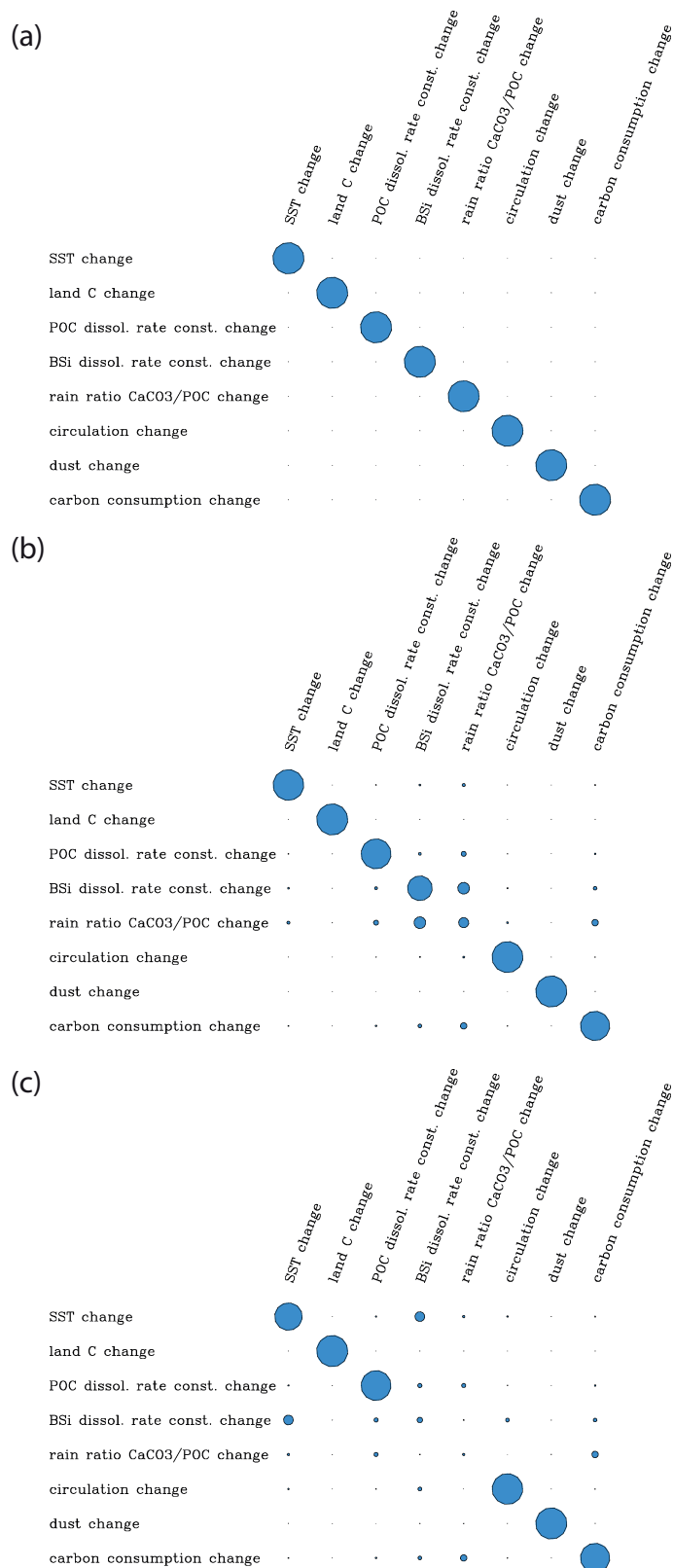
Figure 9. Resolution matrices for the full rank (rank 8) (a), rank 7 (b), and rank 6 (c) solutions. The CaCO$_3$:C$_{org}$ rain ratio variations cannot be anymore determined for a realistic length of the solution vector of parameter variations.
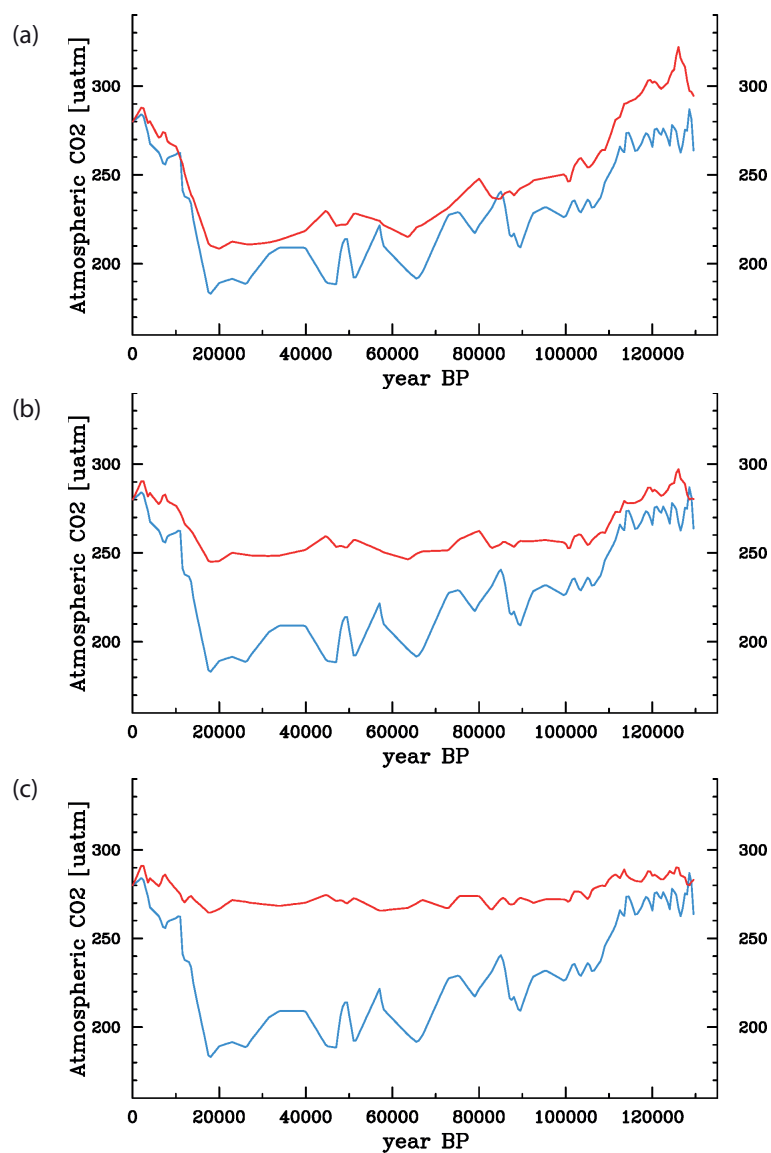
Figure 10. Goodness of fit for the full rank (rank 8) (a), rank 7 (b), and rank 6 (c) solutions (blue line: observations; red line: inverse modelling result). The example is for the predicted evolution of atmospheric CO_2. The observed record comes from the Vostok ice core, Antarctica (Barnola et al., 1987). The rendering of realistic parameter variations in the rank deficient solutions is accompanied by a strong reduction in goodness of fit.

Table 1. Global bulk numbers for the model control run.

Global Value	Control Run Value
atmospheric pCO$_2$ [μatm]	284.0
POC export production [PgC/yr]	9.60
POC deposition to sediment [PgC/yr]	0.088
POC accumulation in sediment [PgC/yr]	0.060
POC accumulation in sediment [teramole C/yr]	5.000
CaCO$_3$ export production [PgC/yr]	1.72
CaCO$_3$ deposition [PgC/yr]	0.37
CaCO$_3$ accumulation [PgC/yr]	0.32
CaCO$_3$ accumulation [teramole C/yr]	27.0
opal export production [teramole Si/yr]	251
opal deposition [teramole Si/yr]	13.7
opal accumulation [teramole Si/yr]	4.5

Table 2. Parameter changes x_j, j=1, …, n; n=8 as imposed in the sensitivity experiments with the full 3-D biogeochemical model relative to the control run parameter choice. The x_j are the maximum amplitude of change for the respective strongest excursion of the observed δD curve at the LGM.

j	parameter description	value of param. change x_j
1	sea surface temperature for computation of the chemical and biological constants:	-5°
2	loss in carbon stock of the terrestrial biosphere:	-1000 PgC
3	dissolution rate constants of POC:	-10%
4	dissolution rate constants of BSi:	-10%
5	export production rain ratio $CaCO_3$:POC:	-10%
6	3-D oceanic velocity field:	100% glacial field
7	glacial dust deposition and associated stimulation of biological export production:	100% glacial field
8	Redfield ratio C:P:	+15%

Table 3. Marine sediment core data and ice core data which were used for determining the parameter changes through a fit of the linear response model. References in parentheses denote the original source of the data in case the data has been taken from a compilation.

Core name	area	lat. +N, -S	long. -W, +E	depth [m]	record used	reference
Vostok	Antarctica	-78	-106	-3488	at. CO_2	Barnola et al. (1987)
M13519	Eq. Atlantic	5.333	-19.183	n.giv.	$\delta^{13}C_{benthic}$	Sarnthein et al. (1984)
RC13-1110	Eq. Pacific	0.100	-95.650	3231	$\delta^{13}C_{benthic}$	Mix (1991)
EW9209-1JP	N. Atlantic	5.0	-43.0	4056	$\delta^{13}C_{benthic}$	Oliver et al. (2010) (Curry and Oppo (1997))
GEOB1115-3	S. Atlantic	-3.56	-12.56	2945	$\delta^{13}C_{benthic}$	Oliver et al. (2010) (Bickert and Wefer (1996))
GEOB1721-6	S. Atlantic	-29.17	13.08	3044	$\delta^{13}C_{benthic}$	Oliver et al. (2010) (Bickert and Mackensen (1996))
GEOB1722-3	S. Atlantic	-29.49	11.75	3073	$\delta^{13}C_{benthic}$	Oliver et al. (2010) (Mollenhauer et al. (2002))
GIK13519-1	N. Atlantic	5.67	-19.85	2862	$\delta^{13}C_{benthic}$	Oliver et al. (2010) (Sarnthein et al. (1994))
GIK23414-9	N. Atlantic	53.54	-20.29	2196	$\delta^{13}C_{benthic}$	Oliver et al. (2010) (Jung and Sarnthein (2003c))
GIK23415-9	N. Atlantic	53.18	-19.14	2472	$\delta^{13}C_{benthic}$	Oliver et al. (2010) (Jung and Sarnthein (2003d))
KNR140-37J	N. Atlantic	31.41	-75.26	3000	$\delta^{13}C_{benthic}$	Oliver et al. (2010) (Keigwin (2004))
ODP1087	S. Atlantic	-31.46	15.31	1372	$\delta^{13}C_{benthic}$	Oliver et al. (2010) (Pierre et al. (2004))
GEOB3004-1	Indian Oc.	14.61	5292.	1803	$\delta^{13}C_{benthic}$	Oliver et al. (2010) (Schmiedl and Mackensen (2006))
MD01-2378	Indian Oc.	-13.08	121.79	1783	$\delta^{13}C_{benthic}$	Oliver et al. (2010) (Kawamura et al. (2006))
MD97-2121	S. Pacific	-40.38	177.99	3014	$\delta^{13}C_{benthic}$	Oliver et al. (2010) (Carter et al. (2008))
M13519	Eq. Atlantic	5.333	-19.183	n.giv.	$\delta^{13}C_{planktonic}$	Sarnthein et al. (1984)
V19-30	Eq. Pacific	-3.350	-83.350	3091	$\delta^{13}C_{planktonic}$	Shackleton and Pisias (1985)
GIK17049-6	N. Atlantic	55.26	-26.73	3331	$\delta^{13}C_{planktonic}$	Oliver et al. (2010) (Jung and Sarnthein (2004))
GIK23415-9	N. Atlantic	53.18	-19.14	2472	$\delta^{13}C_{planktonic}$	Oliver et al. (2010) (Jung and Sarnthein (2003a))
GIK23418-8	N. Atlantic	52.55	-20.33	1491	$\delta^{13}C_{planktonic}$	Oliver et al. (2010) (Jung and Sarnthein (2003b))
ODP1089	S. Atlantic	-40.94	9.89	4621	$\delta^{13}C_{planktonic}$	Oliver et al. (2010) (Hodell et al. (2003b))
RC13-138	Eq. Pacific	1.81	-94.14	2655	$\delta^{13}C_{planktonic}$	Oliver et al. (2010) (Delphiprojekt, Dürkoop et al. (1997)
C4402	W Pacific	2.996	135.022	4402	BSi	Kawahata et al. (1998)
H3571	N Pacific	34.904	179.703	3571	BSi	Kawahata et al. (2000)
RC24-07	Eq. Atlantic	-1.350	-11.917	3899	BSi	Verardo and McIntyre (1994)
503B	E. Eq. Pac.	4.8	-95.6	3672	BSi	Rea et al. (1986)

Table 4. Marine CaCO$_3$ sediment core data which were used for determining the parameter changes through a fit of the linear response model. References in parentheses denote the original source of the data in case the data has been taken from a compilation.

Core name	area	lat. +N, -S	long. -W, +E	depth [m]	record used	reference
C4402	W Pacific	2.996	135.022	4402	CaCO$_3$-wt.%	Kawahata et al. (1998)
GC342	S Pacific	-45.100	147.743	4002	CaCO$_3$-wt.%	Moy et al. (2006)
H3571	N Pacific	34.904	179.703	3571	CaCO$_3$-wt.%	Kawahata et al. (2000)
MD972106	S Pacific	-45.148	146.285	3310	CaCO$_3$-wt.%	Moy et al. (2006)
ODP980	N Atlantic	55.485	-14.702	2168	CaCO$_3$-wt.%	Hyun et al. (2005)
RC24-07	Eq. Atlantic	-1.350	-11.917	3899	CaCO$_3$-wt.%	Verardo and McIntyre (1994)
WEC8803B-GC51	Eq. Pacific	1.300	-133.600	4410	CaCO$_3$-wt.%	LaMontagne et al. (1996)
RC11-210	Eq. Pacific	1.8	-140.0	4420	CaCO$_3$-wt.%	Chuey et al. (1987)
503B	E. Eq. Pac.	4.8	-95.6	3672	CaCO$_3$-wt.%	Rea et al. (1986)
114-704A	S. Atlantic	-46.879	7.421	2543	CaCO$_3$-wt.%	Hoogakker et al. (pers. comm.)(Hodell (1993))
GeoB1032-3	S. Atlantic	-22.915	6.037	2502	CaCO$_3$-wt.%	Hoogakker et al. (pers. comm.)(Bickert (1992); Bickert and Wefer (1996))
GeoB1034-3	S. Atlantic	-21.735	5.422	3772	CaCO$_3$-wt.%	Hoogakker et al. (pers. comm.) (Bickert (1992); Bickert and Wefer (1996))
GeoB1035-4	S. Atlantic	-21.587	5.028	4453	CaCO$_3$-wt.%	Hoogakker et al. (pers. comm.) (Bickert (1992); Bickert and Wefer (1996))
GeoB1041-3	Eq. Atlantic	-3.475	-7.60	4033	CaCO$_3$-wt.%	Hoogakker et al. (pers. comm.) (Bickert (1992); Bickert and Wefer (1996); Mackensen and Bickert (1999))
GeoB1105-4	Eq. Atlantic	-1.665	-12.428	3225	CaCO$_3$-wt.%	Hoogakker et al. (pers. comm.) (Bickert (1992); Bickert and Wefer (1996); Mackensen and Bickert (1999))
GeoB1112-4	S. Atlantic	-5.778	-10.750	3125	CaCO$_3$-wt.%	Hoogakker et al. (pers. comm.) (Bickert (1992); Bickert and Wefer (1996); Mackensen and Bickert (1999))
GeoB1115	Eq. Atlantic	-3.562	-12.560	2945	CaCO$_3$-wt.%	Hoogakker et al. (pers. comm.)(Bickert (1992); Bickert and Wefer (1996); Mackensen and Bickert (1999))
GeoB1117-2	Eq. Atlantic	-3.815	-14.897	3984	CaCO$_3$-wt.%	Hoogakker et al. (pers. comm.)(Bickert (1992); Bickert and Wefer (1996); Mackensen and Bickert (1999))
GeoB1118	Eq. Atlantic	-3.560	-16.428	4671	CaCO$_3$-wt.%	Hoogakker et al. (pers. comm.)(Bickert (1992); Bickert and Wefer (1996); Mackensen and Bickert (1999))
GeoB1211-3	S. Atlantic	-24.475	7.533	4084	CaCO$_3$-wt.%	Hoogakker et al. (pers. comm.)(Bickert (1992); Bickert and Wefer (1996); Mackensen and Bickert (1999))
GeoB1214-1	S. Atlantic	-24.690	7.240	3210	CaCO$_3$-wt.%	Hoogakker et al. (pers. comm.)(Bickert (1992); Bickert and Wefer (1996))
GeoB1505-2	Eq. Atlantic	2.267	-33.015	3706	CaCO$_3$-wt.%	Hoogakker et al. (pers. comm.)(Zabel et al. (1999))
GeoB1710-3	S. Atlantic	-23.432	11.698	2987	CaCO$_3$-wt.%	Hoogakker et al. (pers. comm.)(Schmiedl and Mackensen (1997): Kirst et al. (1999); Kirst (1998))
GeoB1711-4	S. Atlantic	-23.315	12.377	1967	CaCO$_3$-wt.%	Hoogakker et al. (pers. comm.)(Little et al. (1997); Müller (2006))
GeoB3935-2	N. Atlantic	12.613	-59.387	1558	CaCO$_3$-wt.%	Hoogakker et al. (pers. comm.)(Schlünz et al. (2000); Schlunz et al. (2000))
GeoB3938	N. Atlantic	12.588	-58.098	2467	CaCO$_3$-wt.%	Hoogakker et al. (pers. comm.)(Schlünz (1998); Schlunz et al. (2000))
GeoB4240-2	N. Atlantic	28.888	-13.225	1358	CaCO$_3$-wt.%	Hoogakker et al. (pers. comm.)(Freudenthal et al. (2002); Freudenthal (1998))
MD95-2039	N. Atlantic	40.578	-10.349	3381	CaCO$_3$-wt.%	Hoogakker et al. (pers. comm.)(Thomson et al. (2000); Thomson et al. (1999); Zahn et al. (1997))
MD96-2080	S. Atlantic	-36.267	19.475	2488	CaCO$_3$-wt.%	Hoogakker et al. (pers. comm.)(Rau et al. (2002))
ODP1088	S. Atlantic	-41.136	13.563	2082	CaCO$_3$-wt.%	Hoogakker et al. (pers. comm.)(Hodell et al. (2003a))
ODP1089	S. Atlantic	-40.936	9.894	4620	CaCO$_3$-wt.%	Hoogakker et al. (pers. comm.)(Hodell et al. (2003a))
PS2082	S. Atlantic	-43.220	11.738	4610	CaCO$_3$-wt.%	Hoogakker et al. (pers. comm.)(Mackensen et al. (1994))
PS2489-2	S. Atlantic	-42.870	8.970	3794	CaCO$_3$-wt.%	Hoogakker et al. (pers. comm.)(Kuhn (1999); Becquey and Gersonde (2002); Becquey and Gersonde (2003))
RC13-228	S. Atlantic	-22.330	11.198	3204	CaCO$_3$-wt.%	Hoogakker et al. (pers. comm.)(Ruddiman and Farrell (1996a); Curry et al. (1988))
TTN057-6	S. Atlantic	-42.913	8.600	3751	CaCO$_3$-wt.%	Hoogakker et al. (pers. comm.)(Hodell et al. (2003a))
V22-108	S. Atlantic	-43.180	-3.250	4171	CaCO$_3$-wt.%	Hoogakker et al. (pers. comm.)(Charles et al. (1991))
V25-59	Eq. Atlantic	1.370	-33.480	3824	CaCO$_3$-wt.%	Hoogakker et al. (pers. comm.)(Imbrie et al. (1989))
V30-97	N. Atlantic	41.000	-32.930	3371	CaCO$_3$-wt.%	Hoogakker et al. (pers. comm.)(Ruddiman et al. (1989); McIntyre and Imbrie (2000); McIntyre (1989); Ruddiman and Farrell (1996b))
ELT49018-PC	Indian Oc.	-46.050	90.155	3282	CaCO$_3$-wt.%	Hoogakker et al. (pers. comm.)(Howard and Prell (1992))
RC11-120	Indian Oc.	-43.520	79.867	3193	CaCO$_3$-wt.%	Hoogakker et al. (pers. comm.)(Martinson et al. (1987))
CHat01k	S. Pacific	-41.583	171.500	3556	CaCO$_3$-wt.%	Hoogakker et al. (pers. comm.)(McCave et al. (2008); Lean and McCave (1998))
CHat3k	S. Pacific	-42.660	167.496	4802	CaCO$_3$-wt.%	Hoogakker et al. (pers. comm.)(McCave et al. (2008))
CHat5k	S. Pacific	-40.783	171.549	4240	CaCO$_3$-wt.%	Hoogakker et al. (pers. comm.)(McCave et al. (2008))
DSDP594	S. Pacific	-45.523	174.948	1204	CaCO$_3$-wt.%	Hoogakker et al. (pers. comm.)(McCave et al. (2008);)
H3571	N. Pacific	34.904	179.703	3571	CaCO$_3$-wt.%	Hoogakker et al. (pers. comm.)(Kawahata et al. (2000))
NGC108	N. Pacific	36.514	158.348	3390	CaCO$_3$-wt.%	Hoogakker et al. (pers. comm.)(Maeda et al. (2002)
RC13-115	Eq. Pacific	-1.652	-104.800	3621	CaCO$_3$-wt.%	Hoogakker et al. (pers. comm.)(Lyle et al. (2002)
TT013-PC72	Eq. Pacific	0.114	-139.402	4298	CaCO$_3$-wt.%	Hoogakker et al. (pers. comm.)(Murray et al. (2000))
V19-27	Eq. Pacific	-0.467	-82.070	1373	CaCO$_3$-wt.%	Hoogakker et al. (pers. comm.)(Lyle et al. (2002)
V19-28	Eq. Pacific	-2.367	-84.650	2720	CaCO$_3$-wt.%	Hoogakker et al. (pers. comm.)(Lyle et al. (2002)
V19-30	Eq. Pacific	-3.383	-83.520	2091	CaCO$_3$-wt.%	Hoogakker et al. (pers. comm.)(Ninkovich and Shackleton (1975); Shackleton and Pisias (1985))
W8402-14GC	Eq. Pacific	0.953	-138.955	4287	CaCO$_3$-wt.%	Hoogakker et al. (pers. comm.)(Lyle et al. (2002)
Y69-71	Eq. Pacific	0.000	-86.000	2740	CaCO$_3$-wt.%	Hoogakker et al. (pers. comm.)(Pisias and Mix (1997))
Y71-9-101	S. Pacific	-6380	-106.520	3175	CaCO$_3$-wt.%	Hoogakker et al. (pers. comm.)(Lyle et al. (2002); Pisias and Mix (1997))

Table 5. Maximum parameter changes at last glacial maximum relative to interglacial control run.

Run specification	SST [°]	land C storage [PgC]	POC dissol. rate [%]	BSi dissol. rate [%]	rain ratio change CaCO3:C_{org} [%]	circulation change on [%]	dust change on [%]	carbon over-consumption change [units C rel. to P]
Full rank 8	-6.017	-416.7	5.131	3.047	-34.29	48.21	7.861	28.32
Rank 7	-7.894	-441.7	-1.171	-11.85	-7.438	25.88	9.39	10.51
Rank 6	-4.938	-438.3	-0.156	2.373	1.685	45.95	12.34	10.50

Table 6. Average goodness of fit expressed as root mean square error for the control run base line and the different optimisations. The values for the optimisations are estimated from the linear fitting procedure.

Run specification	All records [normalised units]	Atmosp. CO_2 [ppm]	$\delta^{13}C$ benthic [‰]	$\delta^{13}C$ planktonic [‰]	BSi [wt-%]	CaCO$_3$ [wt-%]
Control run	0.4636	61.02	0.3515	0.5515	4.454	15.10
Full rank 8	0.3519	21.05	0.2443	0.4507	4.059	14.39
Rank 7	0.3559	38.59	0.2452	0.4804	3.982	14.66
Rank 6	0.3580	53.25	0.2446	0.4782	4.052	14.94

Table 7. Average rms deviation of the optimised modelled tracer records (as estimated from the simultaneous fit of the sensitivity experiment results to the observations) from the simulated control run tracer record. A zero value would mean that no difference with respect to the control run has occurred. The larger the values, the more differ the optimised tracer curves from the control run, i.e. zero change, case.

Run specification	Atmosp. CO_2 [ppm]	$\delta^{13}C$ benthic [‰]	$\delta^{13}C$ planktonic [‰]	BSi [wt-%]	CaCO$_3$ [wt-%]
Full rank 8	46.12	0.2471	0.3514	1.497	6.062
Rank 7	23.49	0.2465	0.3831	1.090	4.752
Rank 6	8.887	0.2480	0.3595	1.070	3.554

Table A1. Model parameter values as set for the control or standard run.

Tunable Model Parameter	parameter symbol	Control Run Value
specific gas exchange rate for CO_2	k_{CO2}	0.0603 [mole/(m^2·yr·ppm)]
O_2 gas transfer velocity	k_{O2}	250 [m/yr]
threshold value S_{opal} of particle export production ratio C(opal):C(POC) for the onset of CaCO$_3$ production (see eq. 5)		0.6
maximum possible production rain ratio C(CaCO$_3$):C(POC) (see eq. 12)	R	0.375
global weathering input of Si	-	$4.5 \cdot 10^{12}$ [mole Si yr-1]
global weathering input of CaCO$_3$	-	$27 \cdot 10^{12}$ [mole C yr^{-1}]
global weathering input of POC	-	$5 \cdot 10^{12}$ [mole C yr^{-1}]
Si(OH)$_4$ saturation concentration	C_{sat}	800 [μmole yr^{-1}]
degradation rate constant of CaCO$_3$ in water column	r_{CaCO3}	6.76 [yr^{-1}]
minimum value for CaCO$_3$ undersaturation in water column	Ω_{min}	0.062
degradation rate constant of opal in water column	r_{opal}	1.23 [yr^{-1}]
degradation rate constant of POC in water column	r_{POC}	2.69 [yr^{-1}]
sinking velocity of particulate matter in water column	w_M	3 m/day
degradation rate constant for dissolved organic carbon in the water column		0.05 [yr^{-1}]
degradation rate constant of CaCO$_3$ in sediment	r^*_{CaCO3}	$6.55 \cdot 10^{-4}$ / C$_{sat,CaCO3}$ [yr^{-1} l mole^{-1}]
degradation rate constant of opal in sediment	r^*_{opal}	$9.82 \cdot 10^{-4}$ / C$_{sat,opal}$ [yr^{-1} l mole^{-1}]
degradation rate constant of organic carbon in sediment	r^*_{orgC}	$2.69 \cdot 10^{-4}$ / C$_{sat,opal}$ [yr^{-1} l mole^{-1}]
diffusion constant for pore waters	D_w	$8 \cdot 10^{-6}$ [cm^2/s]
coefficient for explicit bioturbation	D_b	40 [cm^2/1000yr]